Generalized Taylor-Aris dispersion in discrete spatially periodic networks: Microfluidic applications

Kevin D. Dorfman and Howard Brenner*
Department of Chemical Engineering, Massachusetts Institute of Technology, Cambridge, Massachusetts 02139
(Received 22 August 2001; published 14 January 2002)

A theory is presented for the lumped parameter, convective-diffusive transport of individual, noninteracting Brownian solute particles (''macromolecules'') moving within spatially periodic, solvent-filled networks—the latter representing models of chip-based microfluidic chromatographic separation devices, as well as porous media. Using graph-theoretical techniques, the composite medium is conceptually decomposed into a network of channels (the edges) through which the solute is transported by a combination of molecular diffusion and either ''piggyback'' entrainment within a flowing solvent or an externally applied force field acting upon the solute molecules. A probabilistic choice of egress channel for a solute particle exiting the intersection (vertex) of the channels is furnished by an imperfect mixing model. A spatially periodic, Taylor-Aris-like ''method-of-moments'' scheme is applied to this transport model, leading to discrete matrix equations for computing the network-scale particle velocity vector $\overline{\mathbf{U}}^*$ and dispersivity dyadic $\overline{\mathbf{D}}^*$ in terms of the prescribed microscale transport parameters and network geometry characterizing the basic unit cell of which the spatially periodic device is comprised. The ensuing algebraic equations governing the vertex-based, discrete unit-cell ''fields'' $P_0^\infty(i)$ and $\mathbf{B}(i)$ $(i=1,2,...,n)$, whose paradigmatic summations yield $\overline{\mathbf{U}}^*$ and $\overline{\mathbf{D}}^*$, constitute *discrete* analogs of classical *continuous* macrotransport phenomenological parameters, $P_0^\infty(\mathbf{r})$ and $\mathbf{B}(\mathbf{r})$, with $\mathbf{r}$ a *continuous* position vector defined within the unit cell. The ease with which these discrete calculations can be performed for complex networks renders feasible parametric studies of potential microfluidic chip designs, particularly those pertinent to biomolecular separation schemes. Application of this discrete theory to the dispersion analysis of pressure-driven flow in spatially periodic serpentine microchannels is shown to accord with existing results previously derived using classical continuous macrotransport theory.

DOI: 10.1103/PhysRevE.65.021103 PACS number(s): 05.40.Jc, 07.10.Cm, 47.55.Mh

I. INTRODUCTION

Engineering design and analysis of spatially periodic microfluidic separation devices requires characterizing the functional dependence of chip-scale (L-scale) mean solute transit rates across the device upon the prescribed interstitial-scale (l-scale; $l \ll L$) parameters quantifying the repetitive unit-cell configuration and local transport properties of the several distinct (macromolecular) solutes to be separated as these molecules traverse the fluid-filled interstitial space. As is often the case in such modeling schemes, a rigorous, pointwise (''continuous'') description of the l-scale transport within the network tends to be exceedingly difficult (if at all possible), owing in large measure to incomplete knowledge of the detailed mechanisms quantifying the transport of flexible polymeric or biological molecules within constraining geometries. Consequently, the rigor implicit in any continuous model for predicting the L-scale solute transport across the chip as a whole, such as is embodied in classical generalized Taylor dispersion theory [1], is often negated by the need to invoke coarse, *ad hoc* assumptions regarding the physical nature of the local solute transport processes, such as employing a (scalar) mean electrophoretic solute mobility in lieu of the exact pointwise mobility dyadic. The present paper aims to incorporate, *a priori*, all of our ignorance of the detailed phenomenology underlying these local issues into a discrete network theory, rendering the latter analytically and computationally tractable when compared with the more rigorous continuous descriptions [1] of such spatially periodic networks.

The analysis which follows is focused primarily upon modeling microfluidic chromatographic separation devices embossed on chips. In the context of chromatographic separations, such micropatterned media find ready application as vector chromatographic separation devices [2], wherein the distinct species undergo simultaneous directional and temporal separation. By ''directional'' is meant that, on the L scale, different species move in different directions in response to the animating force. In contrast, ''temporal'' separation refers to the fact that even if the several species move, on average, in the same direction, they generally do so at different *speeds*, thereby effecting their separation in time, such as occurs in conventional scalar (or unidirectional) chromatography. Experiments performed on such micropatterned devices have demonstrated the efficient separation of variable-length DNA strands [3,4].

Previous attempts to model such directional separation phenomena include our application of rigorous continuous Taylor-Aris dispersion theory [2] and a preliminary version [5] of the present theory, as well as more intuitive models [6,7] developed by others. In addition to being directly applicable to the phenomenon of vector chromatography, the generic theory to be developed herein lends itself to applications involving other classes of microfluidic separation devices, such as magneto-sensitive arrays [8] and en-

*Email address: hbrenner@mit.edu.

tropic trapping devices [9], as well as furnishing an elementary model for transport in porous media. Applications of the present theory to these specific devices is deferred to future installments.

To the extent that Taylor-Aris dispersion theory [1] provides an adequate description of the global aspects of the solute transport processes occurring within the network, only two parameters are required to quantify the average *L*- or chip-scale solute transport rates: (i) the mean solute velocity vector $\overline{\mathbf{U}}^*$, representing the coefficient of the asymptotic *L*-scale linear temporal growth in time of the mean vector displacement of the solute particle from the point of its initial introduction into the network; and (ii) the solute dispersivity dyadic $\overline{\mathbf{D}}^*$, comparably representing the corresponding growth in time of the solute's mean-squared dyadic deviation from its current mean position. The vector velocity difference $\overline{\mathbf{U}}_1^* - \overline{\mathbf{U}}_2^*$ between two distinct solute ''molecules'' or species 1 and 2, introduced simultaneously, quantifies the relative separation occurring between them as they traverse the network. Similarly, the respective particle dispersivities, say, $\overline{\mathbf{D}}_1^*$ and $\overline{\mathbf{D}}_2^*$, serve to characterize the extent of band broadening of these solutes, arising from the stochastic nature of the solute transport processes occurring within the network.

Network models, albeit typically devoid of rigorous Taylor-Aris foundations, have been applied previously to a vast array of practical problems, including transport in porous media [10–20] and fractal models thereof [21–23], deep-bed filtration [24,25], soil science [26,27], and various chromatographic separation schemes [28–30]. Early work in these fields is reviewed by van Brakel [31]. To date, the majority of these network analyses have focused primarily upon dispersion in random porous media [12,16–20,27,32,33], or upon the inherent disorder prevailing in packed bed chromatographic separation devices [28–30], with much attention focused upon the solute dispersivity in such networks near the percolation threshold [17,20,25,27,34]. Moreover, network models [10–17,19,21–23,25,27,30,32,33] have heretofore dealt mostly with unidirectional, pressure-driven, piggyback solute transport through the network. In such circumstances, the mean particle motion has invariably been regarded as being colinear with the Darcy-scale (*L*-scale) solvent pressure gradient, a phenomenon which is not generally true of vector chromatographic separations.

In contrast with all but two [14,22] of the preceding network analyses, we here apply a rigorous Taylor-Aris-like ''method-of-moments'' *L*-scale scheme to the lumped parameter, *l*-scale transport processes occurring within the spatially periodic network [35]—ultimately deriving a generic paradigm for calculating the physically relevant macroscopic parameters, namely $\overline{\mathbf{U}}^*$ and $\overline{\mathbf{D}}^*$, from knowledge of the prescribed *l*-scale data. Building upon the discrete framework of Adler and Brenner [14], the present contribution relaxes their assumption of perfect mixing at the intersections of the individual channels, in addition to incorporating molecular diffusion within the channels into the analysis. With the exceptions [14,22] cited above, our discretization contrasts with existing generalized Taylor-Aris dispersion theory analyses [1], which are predicated upon a precise, pointwise, continuous description of the *l*-scale transport phenomena occurring in spatially periodic media. Accordingly, the generalized Taylor-Aris dispersion paradigm developed herein represents a complete discretization of the comparable classical continuous paradigm [36]—the present graph-theoretical framework being motivated by the creation of classes of perfectly periodic chromatographic devices [3,4,8,9]. Moreover, the concomitant difficulties posed by the geometric complexities of such microfluidic devices [2] motivates the subsequent use of experimentally measurable, albeit averaged, discrete *l*-scale transport parameters in place of classical continuous *l*-scale transport data.

All network models, including ours, proceed in a similar fashion, initially requiring three *l*-scale data inputs pertaining to: (i) the *l*-scale description of the entraining solvent flow field, such as that determined by an electrical resistance analog [12,13,21,23] for fluid motion animated by a Darcy-scale pressure gradient; (ii) the *l*-scale solute transport parameters, namely, the mean, interstitial-level particle velocity vector and diffusivity (dispersivity) dyadic prevailing within the individual channels of the network; and (iii) the selection of a so-called ''mixing'' rule characterizing the choice of solute intersectional exiting protocol from the channel junctions wherein the *l*-scale channel contents coalesce.

Disagreement exists in the network modeling literature concerning delineation of the *l*-scale (effective) intrachannel transport processes, with existing models employing either molecular properties [16,27,34] or effective Taylor-Aris dispersion properties [17,18,20,28,29,33]. As such, it behooves us to amplify, during the course of the subsequent analysis, the relationship existing between the effective intrachannel solute velocity and diffusivity (dispersivity) and the comparable pointwise particle velocity vector and molecular diffusivity dyadic appearing in the continuous scheme. The latter pair of microtransport parameters, $\mathbf{U}(\mathbf{r})$ and $\mathbf{D}(\mathbf{r})$, are, in principle, exactly expressible functionally in terms of the continuous *l*-scale local particle position vector $\mathbf{r}$ within the repetitive unit cell. In contrast, because of their coarser discrete *l*-scale nature, the effective channel transport parameters, $\mathbf{U}(j)$ and $\mathbf{D}(j)$, cannot be known exactly owing to uncertainty existing in the instantaneous local position $\mathbf{r}$ of the particle within channel *j*, arising from the stochastic nature of the molecular diffusive transport processes. For example, the transport of an entrained (point-size) particle by a parabolic Poiseuille flow field may take place entirely along the channel center, resulting thereby in a mean channel velocity significantly greater than that for a particle moving proximate to the channel walls. Such effects become more pronounced in the context of finite-size particles, wherein hydrodynamic wall effects induced by the finite size of the particles relative to the channel width [37] must be incorporated into the analysis [38]. This is especially true in the case of force-driven particle animation or electro-osmotic flow [41], where wall effects constitute the *only* mechanism enabling particle vector separation. The possibility that a particle will statistically sample the entire cross-sectional area of a given channel before exiting that channel, as required for

Taylor-Aris theory to be applicable, necessarily decreases monotonically with the channel's longitudinal dimension—increasing thereby the likelihood of the particle spending a statistically inordinate time resident on a given streamline, or too long in a region of unchanging mobility in the finite-size particle case. Even more tenuous than in the preceding case of modeling the solute velocity in a channel is the issue of properly defining the channel dispersivity, given that the presence of convection gives rise to a Taylor contribution to that effective diffusivity [42], which formula, however, is strictly valid only for relatively long tubes, or, more precisely, for large aspect ratio channels.

A comprehensive study [30] incorporating various effective transport models, both theoretical and semiempirical, found the ensuing *L*-scale macrotransport parameters to be only weakly dependent upon the choice of transport model, but strongly dependent upon the connectivity of the network. In spite of this potentially weak dependence in certain circumstances, it nevertheless behooves us to formulate rational definitions for the effective channel transport parameters, especially in the asymptotic limit (cf. Sec. V A 1).

Numerous models also exist for quantifying the solute ''mixing'' processes occurring at the channel junctions. Unlike the mean intrachannel transport parameters, the mixing rule, serving to quantify the probability of the particle exiting the intersection through a specified channel among those available, is less equivocal, being governed by the physics of the device. Most widely used is the ''perfect mixing'' hypothesis [14,16–19,28–30,33,34], wherein no bias is assumed to exist regarding the choice of intersectional egress channel, owing either to purely convective solute transport (mixing-tank model) in the absence of molecular diffusion, or extremely vigorous molecular diffusion—in probabilistic terms, effectively a Markov process [32]. At large Peclet numbers (convection dominated solute transport), the choice of intersection solute egress channel is typically assumed to be simply proportional to the flow rate prevailing within that channel [24,25,32,33]. At small Péclet numbers, where the transport process is diffusion dominated, steric arguments [33] have been invoked to argue that the choice of intersection egress channel is proportional to that channel's cross-sectional area, while for very small intersections it has also been assumed [27] that no streamwise molecular diffusion occurs.

Each of the preceding mixing rules represent approximations, albeit pragmatically useful ones, of the exact solute transport processes occurring at the channel intersections. A more precise determination of egress channel probabilities may be obtained from the exact solution of the prevailing continuous convective-diffusive transport problem, including proper accountings of the detailed fluid flow field and particle dynamics, e.g., hydrodynamic wall effects. The latter scheme has been employed elsewhere for the analysis of blood hematocrit flow through microvasculature [43], as well as for the Stokesian dynamics of fluid-particle-bed interactions in model porous media [44].

No doubt exists that a continuous description of the vertex transport process, when compared with any of the proposed *ad hoc* probabilistic vertex mixing schemes, would furnish more physically accurate results within this discrete theory. However, given the computational resources required to more precisely quantify the detailed intersectional transport processes, it is only incrementally more difficult to solve the original, classical continuous Taylor-Aris dispersion problem [1] itself. Consequently, practical applications of our discrete Taylor-Aris dispersion theory suggest choosing an appropriate vertex mixing rule in order to approximate the true physical processes prevailing therein—rather than attempting to solve the exactly formulated microscale problem posed at the channel intersections.

Having established a particular physical model for the unit cell-level transport processes, a detailed picture of the global particle transport process is generated from such models typically either by: (i) a Monte Carlo scenario [20,27,30,32,33] whereby single-particle (or ''plume'') transport through the network is statistically simulated numerous times; or (ii) a Laplace transform technique [16–18,20,28,29] wherein a unidirectional, unsteady convection-diffusion equation is solved for the continuous solute concentration distribution prevailing in each discrete channel or pore within the entire network. Continuity of these concentrations at all channel intersections in the network, together with an (arbitrary) choice of initial solute injection point within the network as a whole, jointly with conditions at the (finite) boundaries (if any) of the network, provide sufficient conditions in such models for uniquely specifying the overall solute transport problem. The macroscale transport parameters $\overline{\mathbf{U}}^*$ and $\overline{\mathbf{D}}^*$, globally characterizing the process, are then calculated, either from moments of the simulation statistics or from the convective-diffusive solute concentration profile (cf. Sec. III D).

Proponents [16–18,20] of the Laplace transform technique argue that their scheme constitutes an ''exact'' method for ascertaining these macrotransport parameters, having presumably solved for the complete unsteady microscale concentration field extant within each pore of the network following solute injection. As discussed above, some degree of arbitrariness invariably exists as to the applicability of Taylor-Aris *l*-scale dispersivity arguments for calculating the effective particle velocity and diffusivity prevailing over the length of a single channel, a parameter strictly valid only in an *L*-scale asymptotic sense [1,17,45]. For asymptotically long times, our discrete Taylor-Aris dispersion theory, to be derived, represents a much more compact computational scheme for calculating the *L*-scale parameters $\overline{\mathbf{U}}^*$ and $\overline{\mathbf{D}}^*$ when compared with such Laplace transform techniques, since its use does not necessitate initially obtaining the exhaustively detailed time-dependent solution of the underlying unsteady convection-diffusion equations for each pore of the network prerequisite to calculating these parameters. Moreover, our scheme provides, *inter alia*, rigorous criteria governing use of the single channel, *l*-scale Taylor-Aris parameters entering into the subsequent *L*-scale calculation of $\overline{\mathbf{U}}^*$ and $\overline{\mathbf{D}}^*$. Indeed, the ability to quantitatively obtain the macroscopic *L*-scale transport properties of a solute molecule traversing the medium, without the preliminary necessity for solving for the entire exact, time-and initial condition-

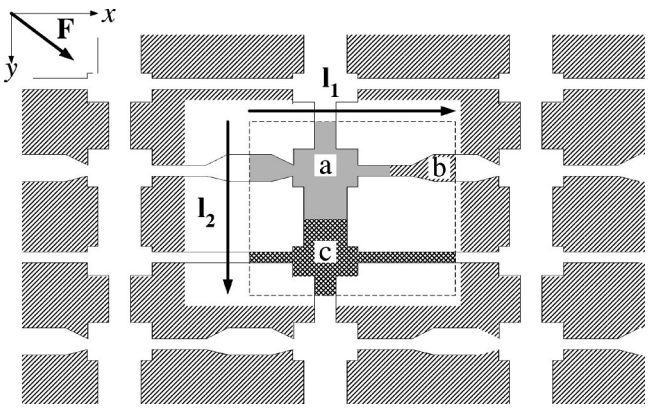

FIG. 1. Schematic of a spatially periodic medium, with solute particle animation effected by the application of an externally applied vector force **F**. The repetitive unit cell is enclosed in the dashed box, with the subsequent discretization of the continuous unit cell regions indicated by the trio of shaded regions labeled *a*, *b*, and *c*. Lattice vectors $\mathbf{l}_1$ and $\mathbf{l}_2$ are indicated.

dependent solute concentration field, constitutes the *raison d'être* underlying macrotransport theory [1].

In this light, we proceed in Sec. II to outline a formal mechanism for converting the fundamental continuous theory for such devices into a more tractable graphical network of the phenomena, continuing in Sec. III with the derivation of a detailed conservation equation for the conditional solute positional and temporal probability density on the graph. Sections IV and V furnish a method-of-moments analysis for the graphical representation of the periodic medium, whereby formulas are derived enabling computation of the respective *L*-scale mean velocity vector and dispersivity dyadic parameters $\overline{\mathbf{U}}^*$ and $\overline{\mathbf{D}}^*$ from the prescribed *l*-scale data. As illustrative examples, transport in serpentine microfluidic channels and ''simple'' networks are examined in Sec. VI. We conclude in Sec. VII with a comparison between the respective continuous and discrete macrotransport theories, including recommendations for applications of the latter.

II. GEOMETRICAL DESCRIPTION

The devices encompassed by our analysis consist of strongly connected, spatially periodic networks of intersecting channels embedded within a three-dimensional space, as depicted in Fig. 1 [46]. By ''strongly connected'' is meant that each fluid point in the medium is accessible to a solute molecule from every other point in the medium. Transport through networks that are not strongly connected may be characterized within the framework of the present scheme by considering the individual Taylor-Aris dispersion processes occurring within each of the separately strongly connected networks which, together, collectively comprise the composite medium [14] as a whole. The spatial periodicity of the network is reflected in the existence of a primitive (parallelepipedal or, if need be, curvilinear) unit cell repeated indefinitely in all directions. The entire composite medium may be imagined as constructed by translating this primitive unit cell (together with its contents) parallel to itself through a trio of basic lattice vectors $(\mathbf{l}_1, \mathbf{l}_2, \mathbf{l}_3)$ satisfying the requirement that their scalar triple product, $\mathbf{l}_1 \cdot \mathbf{l}_2 \times \mathbf{l}_3 = \tau_0$, is equal to the superficial volume τ_0 of the cell [13].

The position of a given cell, say, the **I**th cell, within the three-dimensional space can be identified by specifying the discrete *L*-scale position vector $\mathbf{R}_\mathbf{I}$ of, say, the centroid of the cell relative to an origin, $\mathbf{R}_{\mathbf{I}_0} = \mathbf{0}$, at the centroid of the zeroth cell

$$\mathbf{R}_I = I_1\mathbf{l}_1 + I_2\mathbf{l}_2 + I_3\mathbf{l}_3, \tag{2.1}$$

with (I_1, I_2, I_3) a triplet of positive or negative integers, including zero. The location of the **I**th cell can also be identified by this triplet of integers $\mathbf{I} \equiv (I_1, I_2, I_3)$, itself regarded as a vector or matrix **I**. The exact continuous $l \oplus L$-scale position vector **R**, specifying the location of a point within the three-dimensional space, may be represented by the mixed (discrete, continuous) vector pair $(\mathbf{R}_\mathbf{I}, \mathbf{r}) \equiv \mathbf{R}$, where the *l*-scale continuous vector **r** is the local position vector of a point within any unit cell with respect to that particular cell's centroid. This corresponds to the standard decomposition employed in classical generalized Taylor dispersion theory for spatially periodic media [1,36], in the sense that the subsequently defined $l \oplus L$-scale continuous fields (velocity field, solute concentration field, etc.) are regarded as being exactly defined at each and every fluid point **R** of the $\mathbf{R} \equiv (\mathbf{R}_\mathbf{I}, \mathbf{r})$-space encompassing the entire interstitial fluid region (at each instant in time). This detailed description quantifies the exact, or ''continuous,'' case, in contrast with the subsequent graph-theoretical network treatment (the ''discrete'' case), where fields will be defined only at the discrete points in the subsequently defined $l \oplus L$-scale discrete $\mathcal{I} \equiv (\mathbf{I}, i)$ space, where $i = (1,2,...,n)$ identifies one of the *n* channel intersectional subvolume elements within a unit cell.

A. The basic graph

Significant computational advantages accrue to converting the classical [1,36] continuous **R**-space decomposition of the spatially periodic medium into a discrete $\mathcal{I}$-space graphical representation. The internal configuration of each cell consists of a finite number of intersecting channels, some of which are wholly contained within the unit cell (such as the channel connecting *a* to *b* in the *x* direction of Fig. 1), others being intersected by the unit-cell boundaries (such as the channel connecting *b* to a' in the *x* direction of Fig. 1). The finite basic graph [13] Γ_b is then constructed from the coordination of the channels and their intersections, with the m_b channels in the unit cell comprising the edge set, $j \in E\Gamma_b$, whereas the n_b intersections of the latter edges comprise the vertex set, $i \in V\Gamma_b$. By virtue of the periodicity of the network, there exists within the unit cell two equivalent (homologous) channels intersected by the unit-cell boundary, say, one edge with initial vertex at *i* in cell **I** with terminal vertex at i' in cell $\mathbf{I}'$, and a second edge with initial vertex at *i* in cell $\mathbf{I}''$ and terminal vertex at i' in cell **I**. By convention, we retain only those edges which are directed into the unit cell (with the direction specified forthwith), assigning them the ''macroscopic'' jump vector

$$\mathbf{R}(j) \overset{\text{def.}}{=} \mathbf{R}_{\mathbf{I}} - \mathbf{R}_{\mathbf{I}'}. \tag{2.2}$$

The edge set is characterized completely by each edge's respective orientation and geometry. The orientation of the edge set, which provides an unambiguous definition of the incidence matrix [cf. Eq. (2.6)], as well as classifying the basic graph as a directed graph [47], is chosen such that the scalar convective transport coefficient $c(j)$ is non-negative [cf. Eq. (3.5)] [48]. The latter criterion is satisfied by considering the mean l-scale convective velocity $\langle \mathbf{U}^C \rangle_j$ in edge j imparted to the particle by the entraining fluid flow in the channel, together with the mean l-scale particle velocity $\langle \mathbf{U}^F \rangle_j = \langle \mathbf{M} \rangle_j \cdot \mathbf{F}$ imparted by the action of an externally applied force $\mathbf{F}$ acting on the particle in edge j. Here, $\langle \mathbf{M} \rangle_j$ denotes the mean l-scale solute mobility dyadic in channel j. As in classical macrotransport theory [1], the mean l-scale particle velocity $\langle \mathbf{U} \rangle_j = \langle \mathbf{U}^C \rangle_j + \langle \mathbf{U}^F \rangle_j$ within the edge must be unidirectional, either proceeding spatially from the region represented by vertex i to i', or vice versa. Consequently, the edge is directed such that the edge unit vector $\mathbf{e}(j)$, defined so as to point from the initial to the terminal vertex, is colinear with the mean velocity vector $\langle \mathbf{U} \rangle_j$ in that edge.

While many problems of interest involve channels of uniform cross-sectional configuration, the generic formulation presented herein is not similarly restricted. Regardless of channel tortuosity, it is possible to unequivocally define both a channel volume $v_e(j)$, and channel length $l(j)$, the latter being equal to the distance between the adjacent intersections corresponding to the initial and terminal vertices of edge j. For subsequent calculations requiring a flux per unit area, we define the effective cross-sectional area $A(j)$ of a channel as the ratio of its volume to length

$$A(j) \overset{\text{def.}}{=} \frac{v_e(j)}{l(j)}. \tag{2.3}$$

So as to render explicit the preceding discretization scheme, Fig. 2 depicts the basic graph derived from the continuous medium depicted in Fig. 1, with homologous vertices (i.e., identical vertices present on the basic graph in an adjacent unit cell) denoted by affixing a prime, e.g., a and a'.

The spatially periodic structure of the composite medium is reflected in the global graph [13] Γ_g, which is defined by basic vertices $\{v_i = 1 \leqslant i \leqslant n_b\}$ together with the transformation

$$\mathcal{L} = \{\Lambda + v_i; \;\; 1 \leqslant i \leqslant n_b\}, \tag{2.4}$$

where Λ is the simple lattice corresponding to the base vectors $(\mathbf{l}_1, \mathbf{l}_2, \mathbf{l}_3)$ and $\mathcal{L}$ is the derived lattice. Analogous to the continuous $l \oplus L$-scale $\mathbf{R}$-space description (2.1), the discrete $l \oplus L$-scale $\mathcal{I}$-space global graph is formed by translation through the simple lattice.

B. The local graph

Although the union of the basic graph Γ_b and the transformation of Eq. (2.4) constitutes a complete geometrical discretization of the continuous spatially periodic network,

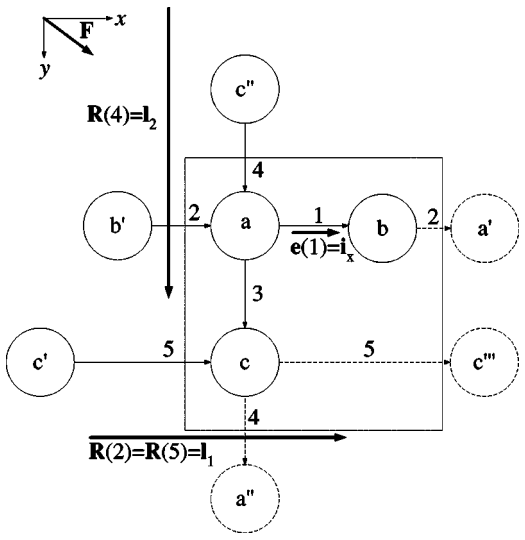

FIG. 2. Basic graph for the spatially periodic medium of Fig. 1, with the unit cell enclosed within the box. The five different types of channels appearing in Fig. 1 are indicated by edge numbers 1 to 5. Homologous vertices existing outside the unit cell are denoted with a prime affix. Edges exiting the unit cell (and their associated homologous vertices), not otherwise included in the basic graph, are indicated by the dashed lines. A representative edge orientation vector $\mathbf{e}(1)$, as well as the macroscopic jump vectors, are depicted. Macroscopic jump vectors for edges wholly contained within the unit cell are zero, i.e., $\mathbf{R}(1) = \mathbf{R}(3) = 0$.

use of the basic graph proves cumbersome in applications, owing to superfluous information implicitly embedded in the homologous vertices. Combining homologous vertices and contracting the additional edges between them furnishes the local graph [13] Γ_l, which will be utilized for all subsequent asymptotic calculations.

Upon contraction, the local graph contains $n \leqslant n_b$ vertices and $m \leqslant m_b$ directed edges. Edges connecting homologous vertices, say, i and i', result in a loop, rendering the local graph nonsimple. In exchange for this nonsimplicity, the local graph is independent of the particular configuration invoked for the basic unit cell [13], as well as requiring minimal computational effort in the subsequent dispersion calculation [49]. For each of the n vertices i on the local graph, assign to the set $j \in \Omega^+(i)$ the subset of those edges j with terminal vertex i, and to the set of edges $j \in \Omega^-(i)$ the subset of those edges j with initial vertex i. From the basic graph of Fig. 2, the latter homologous contraction process furnishes the local graph of Fig. 3, where, for example, $\Omega^+(c) = \{j = 3,5\}$ and $\Omega^-(c) = \{j = 4,5\}$, with the loop obviously a member of both sets.

The unit-cell volume is subdivided in a discrete manner on the local graph to its vertices so as to facilitate exposition of the subsequent ''exactly'' posed description of the solute transport process [cf. Eq. (3.4)] [50]. The volume $v(i)$ of a vertex on the local graph is then defined as being equal to the volume $v_i(i)$ of its channel intersection plus half the volume of all channels incident to that intersection

$$v(i) \overset{\text{def.}}{=} v_i(i) + \tfrac{1}{2} \sum_{j \in \Omega^+(i)} v_e(j) + \tfrac{1}{2} \sum_{j \in \Omega^-(i)} v_e(j). \tag{2.5}$$

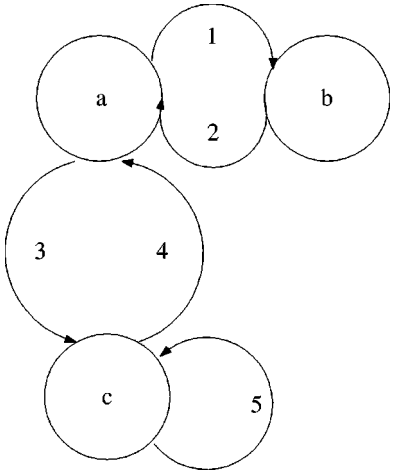

FIG. 3. Local graph constructed from the basic graph of Fig. 2 by combining all homologous vertices and contracting the edges between them. The connectivity between *c*-type vertices results in a loop in the local graph, rendering it nonsimple. The local (x,y) coordinate system is no longer necessary, having been embedded in the macroscopic jump vectors $\mathbf{R}(j)$ and the orientations of the edges.

In addition to assigning the physical volume to a given vertex, we assign the particle's local continuous position $\mathbf{r}$ to the discrete location of vertex i situated, say, at the centroid of the subvolume element $v(i)$, whenever the particle resides within $v(i)$. Consequently, the continuous $\mathbf{R}$-space particle location vector pair $(\mathbf{R_I},\mathbf{r})$ finds its discrete, coarse-grained $\mathcal{I}$-space counterpart in the discrete pair $(\mathbf{I},i)$, the latter corresponding to the particle being located within the volume assigned to vertex i in the unit cell whose centroid is situated at the discrete position $\mathbf{I}$. To complete this discretization, define the l-scale discrete position vector $\mathbf{r}_i$ so as to point from the centroid of cell $\mathbf{I}$ to the centroid of the unit-cell subvolume element $v(i)$ identified by the index i.

C. Pertinent elements of graph theory

In graph-theoretical terms [47] the local graph is a finite-directed graph, composed of the m member edge set $j \in E\Gamma_l$ and the n member vertex set $i \in V\Gamma_l$, thereby permitting the introduction of the $n \times m$ incidence matrix D_{ij} [51]

$$D_{ij} \overset{\text{def.}}{=} \begin{cases} 1 & \text{if vertex } i \text{ is the terminal vertex of edge } j, \\ -1 & \text{if vertex } i \text{ is the initial vertex of edge } j, \\ 0 & \text{otherwise.} \end{cases} \tag{2.6}$$

The rank of the incidence matrix is $n-1$, owing to the connectivity of the graph. It will also prove convenient to decompose the incidence matrix into its positive and negative components,

$$D_{ij} = \Pi_{ij}^{(+)} - \Pi_{ij}^{(-)}, \tag{2.7}$$

where the nonzero entries in $\Pi_{ij}^{(+)}$ are the positive elements of D_{ij}, and the nonzero entries in $\Pi_{ij}^{(-)}$ are the absolute values of the negative elements of D_{ij}.

In what follows, matrix equations for the node-based macrotransport "fields" will be formulated in the cocycle space. Briefly, the cocycle space is constructed by partitioning the vertex space into two connected subgraphs: $V\Gamma = V_1\Gamma \cup V_2\Gamma$. A cocycle H consists of those edges (cuts) with one vertex in subgraph V_1 and a second vertex in subgraph V_2. The vector $\xi_H(e_j)$ associated with cocycle H may be defined as being positive for, say, edges terminating in V_1 [52]

$$\xi_H(e_j) \overset{\text{def.}}{=} \begin{cases} 1 & \text{if } e_j \in H \text{ and its terminal vertex is in } V_1, \\ -1 & \text{if } e_j \in H \text{ and its initial vertex is in } V_1, \\ 0 & \text{otherwise.} \end{cases} \tag{2.8}$$

The $n-1$ cocycles forming the basis of the cocycle space may then be collected into the $m \times (n-1)$ cocycle matrix $\mathbf{K}$. An alternative, more convenient method for constructing $\mathbf{K}$ involves removing the row of the incidence matrix $\mathbf{D}$ that corresponds to the vertex not appearing as a cut set in the fundamental basis of the cocycle space, and then transposing the result. The latter technique, which preserves the structure of the incidence matrix, will be employed in what follows. The cocycle matrix, being of rank $n-1$, furnishes an alternative method to that of the incidence matrix for incorporating the graph connectivity.

III. "EXACTLY" POSED (DISCRETE) PROBLEM

The present section furnishes the conservation equation governing the phenomenological, lumped-parameter description of the solute transport processes occurring at each node of the global graph. We refer to this node-based conservation equation as constituting an "exactly" posed network problem, in the sense that no finer-scale model is contemplated of the unsteady-state transport process undergone by the Brownian solute particle, except, perhaps, for estimating the effective edge transport coefficients in certain limiting circumstances. The subsequent conservation equation represents the discrete counterpart of the continuous $l \oplus L$-scale convective-diffusive equation [cf. Eq. (3.7)] [1], the latter of which serves as the starting point for the method-of-moments homogenization scheme in classical generalized Taylor-Aris dispersion analyses of macrotransport phenomena.

A. Conditional probability density on the global graph

Consider the conditional probability density $P(\mathbf{I}, i, t|\mathbf{I}_0, i_0, t_0)$ of the Brownian particle being located in cell $\mathbf{I}$ within the unit-cell subvolume element represented by vertex i at time t, given its initial introduction at time t_0 into the network in cell $\mathbf{I}_0$ at the vertex i_0 [53]. Given this impulsive introduction of the particle, and choosing $t_0 = 0$ without any loss of generality, conservation of probability density requires that P satisfy the normalization condition

$$\sum_{\Gamma_g} v(i) P(\mathbf{I},\ i,\ t|\mathbf{I}_0,\ i_0) = \begin{cases} 0 & (t \leqslant 0), \\ 1 & (t > 0), \end{cases} \tag{3.1}$$

reflecting the fact that the probability is unity of the particle being located somewhere within the infinitely extended network at any time following its initial introduction.

Since the spatially periodic network is assumed to be generated by translational displacements of the base lattice vectors, or equivalently of the simple lattice [13], it is assumed that the attenuation of P with distance from the point of introduction of the particle into the network is sufficiently rapid to insure that $P \to 0$ as $|\mathbf{I}-\mathbf{I}_0| \to \infty$. Indeed, in order that the summations involved in forming the local moments of P [cf. Eq. (4.1)] converge, as in the continuous case [1], it is further assumed that all moments of the probability density decay faster than algebraically with distance, such that

$$(\mathbf{R}_\mathbf{I}-\mathbf{R}_{\mathbf{I}_0})^m P \to \mathbf{0} \quad \text{as} \quad |\mathbf{I}-\mathbf{I}_0| \to \infty \quad (m=0,1,2,...), \tag{3.2}$$

where, generically, for any vector $\mathbf{V}$, the polyadic $\mathbf{V}^m = \mathbf{VV}\cdots\mathbf{V}$ (m times) is an m-adic.

Of course, real systems are of bounded extent. Consequently, the analysis pursued herein is expected to be valid in the limit where the number N of unit cells in the actual device is large: $N \gg 1$. The latter condition is equivalent to that employed previously in the continuous modeling of micropatterned devices [2], where the infinite system analysis was expected to be valid in the limit $l/L \ll 1$, with l a characteristic dimension of the unit cell and L the characteristic size of the finite macroscopic system as a whole.

As is true for both continuous [1] and discrete [14] unbounded models of spatially periodic systems, P is dependent only upon the global displacement $\mathbf{I}-\mathbf{I}_0$ (or, equivalently, $\mathbf{R}_\mathbf{I}-\mathbf{R}_{\mathbf{I}_0}$) of the particle from its initial position, rather than separately upon both its current and initial positions, $\mathbf{I}$ and $\mathbf{I}_0$, respectively. This fact is equivalent in its consequences to translating the arbitrarily positioned origin, situated at $\mathbf{R}=\mathbf{0}$, to a origin, situated at the point $\mathbf{R}=\mathbf{R}_{\mathbf{I}_0}$. As such, we can arbitrarily choose $\mathbf{I}_0=\mathbf{0}$ and $\mathbf{R}_{\mathbf{I}_0}=\mathbf{0}$ (so that $\mathbf{I}$ and $\mathbf{R}_\mathbf{I}$ are now measured relative to a different origin located within the unit cell into which the particle was originally introduced into the system). Consequently, P possesses the canonical functional form

$$P \equiv P(\mathbf{I},\ i,\ t|i_0). \tag{3.3}$$

B. Microscale transport: Effective properties and mixing rule

A particle navigating the network is assumed to translate through the edges via convection (either ''piggyback'' convection entrained in a flowing fluid or by the action of an externally imposed force field, such as an electric field, or both), as well as by Brownian motion. In constructing the basic graph, the direction of the mean convective transport occurring within the channel, which must of necessity be unidirectional, was embedded in the edge unit vector $\mathbf{e}(j)$. Consequently, transport within the edge is fully characterized by the edge velocity vector, $U(j)\mathbf{e}(j)$, together with the edge diffusivity dyadic, $D(j)\mathbf{e}(j)\mathbf{e}(j)$.

For circumstances in which net solvent motion arises from a Darcy-scale (macroscopic) pressure gradient, the graph-theoretical techniques of Adler and Brenner [13] may be applied directly to the present graphical framework. Alternatively, other network resistance models [12,21,23] may be adopted. Such techniques furnish a coarse-grained approach for calculating the mean fluid velocity prevailing in each of the edges, without requiring detailed knowledge of the finer-scale, **r**-dependent velocity field existing therein. Although the mean *solvent* velocity may thereby be determined unambiguously, establishing the mean *solute* particle velocity $U(j)$ and diffusivity $D(j)$ is considerably more equivocal, as addressed in the Introduction. Within the context of an ''exact'' microscale description of the solute transport process [cf. Eq. (3.4)], the edge transport parameters must then be classified as stochastic variables [54]. It is important, nevertheless, to recognize that despite its stochastic nature, the edge transport process is rendered amenable to rational analysis in the asymptotic Taylor-Aris dispersion limit. Consequently, we will proceed in our ''exact'' analysis using the equivocal, stochastic quantities $U(j)$ and $D(j)$, reserving their unambiguous, *asymptotic* definitions for a later stage of the analysis (cf. Sec. V A 1).

The stochastic nature of our ''exactly'' posed network problem is augmented by the mixing processes occurring in those regions situated at the channel intersections [55]. Explicitly, when the particle is situated in the channel intersection represented by node i, the role of the mixing rule is to furnish the probability of egress channel (edge) j for the particle as it exits intersection i [and, consequently, exits the unit cell subvolume $v(i)$ via edge j]. So as to formulate a generic scheme, applicable to all such network problems, one may envision a set of stochastic vertex-edge probability variables, $0 \leqslant K(i,j) \leqslant 1$, characterizing the probability of the particle entering or exiting the channel represented by edge j from the channel intersection represented by vertex i [56]. However, such a set of variables overspecifies the problem, since the graphical network discretization of the real medium entailed assigning all of the physical volume to the nodes. Consequently, the constraint of zero accumulation of probability density within the volumeless edges is enforced by redefining the mixed vertex-edge parameter K as an edge-based parameter, $K(i,j) \equiv K(j)$. For definiteness, we choose the value of $K(j)$ to correspond to the probability of the particle entering the edge at its initial vertex (i.e., the probability of exiting the vertex in edge j), thereby providing internal consistency with the various mixing-rule schemes enumerated in the Introduction.

The edge probability parameter $K(j)$ possesses an alternate interpretation as a probabilistic ''check valve'' for the vertex. The extreme value $K(j)=0$ corresponds to an edge that is inaccessible to the Brownian particle—say, a conduit of circular cross section whose radius is less than that of the particle (the latter assumed rigid and spherical). Conversely, the extreme value $K(j)=1$ corresponds to a channel into whom solute entry proceeds without bias. It follows that the special value $K(j)=1$ for all edges j reproduces the earlier perfect mixing model of Adler and Brenner [14].

C. Nodal conservation equation

Given the preceding identifications of the local transport processes occurring within the edges and vertices, the fol-

lowing "exact" discrete $l \oplus L$-scale conservation equation governs the conditional probability density that the particle instantaneously, at time t, resides on the global graph at the location $(\mathbf{I},i)$

$$v(i)\frac{dP(\mathbf{I},i)}{dt} = \delta(\mathbf{I})\,\delta(i,i_0)\,\delta(t) + \sum_{\substack{j\in\Omega^+(i)\\ j=\{i',i\}}} c(j)P(\mathbf{I}',\ i') + d(j)[P(\mathbf{I}',\ i') - P(\mathbf{I},\ i)] - \sum_{\substack{j\in\Omega^-(i)\\ j=\{i,i'\}}} c(j)P(\mathbf{I},\ i) + d(j)[P(\mathbf{I},\ i) - P(\mathbf{I}',\ i')], \tag{3.4}$$

with $\delta(\mathbf{I})$ and $\delta(i,i_0)$ Kronecker delta functions, and $\delta(t)$ the Dirac delta function. For notational simplicity, the explicit dependence of P upon both the time t and the initial vertex location i_0 has been suppressed in its argument. The summation index $j\in\Omega^+(i)$ $(j=\{i',i\})$ serves to indicate those edges which enter vertex i from vertex i'. Likewise, $j\in\Omega^-(i)$ $(j=\{i,i'\})$ indicates edges exiting vertex i and proceeding to vertex i'. The non-negative edged-based parameters $c(j)$ and $d(j)$ appearing above correspond to the respective magnitudes of the convective and diffusive "volumetric flow rates" prevailing in edge j [57]

$$c(j) \overset{\text{def.}}{=} K(j)U(j)A(j),\quad d(j) \overset{\text{def.}}{=} \frac{K(j)D(j)A(j)}{l(j)}. \tag{3.5}$$

The equality,

$$\sum_{\substack{j\in\Omega^+(i)\\ j=\{i',i\}}} c(j) = \sum_{\substack{j\in\Omega^-(i)\\ j=\{i,i'\}}} c(j), \tag{3.6}$$

while always true for a solute molecule entrained in a flowing fluid with perfect mixing at intersection i [13], does not necessarily obtain for imperfect mixing or purely force-driven motion. In the former case, the solute mixing bias embodied in the parameter $K(j)$ may negate the equality (3.6); in the latter case, even for perfect mixing and infinitesimally small particles, wherein both K and the (scalar) mobility M are invariant to choice of edge j, the "volumetric flow rate" is not necessarily conserved at an intersection i, say, at which an expansion in channel size occurs, such that $A(j)$ then differs between the two collinear edges incident to vertex i.

The preceding exact discrete $l \oplus L$-scale vertex conservation equation, akin to master equations [58] prevalent in statistical physics, is considerably more *ad hoc* in nature than is its continuous counterpart [cf. Eq. (3.7)], thereby warranting further elaboration of the interpretation ascribed to Eq. (3.4). The left-hand side (LHS) represents the accumulation of probability density within the nodal volume given by Eq. (2.5). The first term on the right-hand side (RHS) represents the unit impulse addition at time $t_0=0$ of solute into unit-cell $\mathbf{I}_0=\mathbf{0}$ within the volume assigned to vertex i_0. The remaining terms, respectively, account for the mechanisms whereby the particle enters and exits the volume assigned to vertex $(\mathbf{I},i)$. Explicitly, convection through the edges transports the particle from the vertex $(\mathbf{I}',i')$ to the vertex $(\mathbf{I},i)$, or, equivalently, removes the particle from vertex $(\mathbf{I},i)$. Terms involving differences, $P(\mathbf{I}',i')-P(\mathbf{I},i)$, in conditional probability densities between connected vertices account for an assumed Fickian-type diffusional process occurring as a consequence of a presumed linear probability gradient existing between the two vertices, the diffusion length scale having been explicitly incorporated *a priori* into the edge transport parameter $d(j)$.

The intractability of the stochastic difference Eq. (3.4) for the graphical network points up a striking contrast between the present discrete formulation and its continuous analog [1]. The comparable exact continuous $l \oplus L$-scale conservation counterpart of Eq. (3.4), governing the conditional probability density $P(\mathbf{R},t|\mathbf{R}_0)\equiv P(\mathbf{R_I},\mathbf{r},t|\mathbf{r}_0)$, possesses the form [1]

$$\frac{\partial P}{\partial t} + \boldsymbol{\nabla}\cdot[\mathbf{U}(\mathbf{r})P - \mathbf{D}(\mathbf{r})\cdot\boldsymbol{\nabla}P] = \delta(\mathbf{R_I})\,\delta(\mathbf{r}-\mathbf{r}_0)\,\delta(t), \tag{3.7}$$

where $\mathbf{U}(\mathbf{r})$ and $\mathbf{D}(\mathbf{r})$ are, respectively, the exactly defined continuous l-scale particle velocity vector and molecular diffusivity dyadic. This latter equation possesses a well-defined mathematical and physical structure, and may be solved, at least in principle, subject to requiring an appropriate spatial rate of attenuation of P with increasing distance from the cell $\mathbf{R}_{\mathbf{I}_0}=\mathbf{0}$ at which the particle was initially introduced. In contrast, the graph-theoretical framework proposed herein possesses no exactly solvable discrete $l \oplus L$-scale formulation, except for circumstances wherein the respective mean edge transport and mixing rules are well defined, i.e., deterministic.

D. Lagrangian definition of the macrotransport parameters $\overline{\mathbf{U}}^*$ and $\overline{\mathbf{D}}^*$

In spite of the stochastic nature of Eq. (3.4), its solution at every node of the global graph furnishes, in principle, the complete set of probability densities $P(\mathbf{I},i,t|i_0)$ on the global graph. With l the characteristic unit-cell linear dimension and D_m the characteristic Brownian particle molecular diffusivity, the asymptotic definitions of the macrotransport parameters $\overline{\mathbf{U}}^*$ and $\overline{\mathbf{D}}^*$ become valid in the long-time limit, $t \gg l^2/D_m$ [1]. Explicitly, with $\mathbf{R}_{\mathcal{I}}\equiv\mathbf{R_I}+\mathbf{r}_i$ the location of the centroid of vertex i in unit-cell $\mathbf{I}$ within which the particle is instantaneously located at time t, the solution of Eq. (3.4) for P permits calculation of the mean particle velocity vector $\overline{\mathbf{U}}^*$ as the average displacement of the Brownian particle with respect to its initial position $\mathbf{R}_{\mathcal{I}_0}\equiv\mathbf{0}+\mathbf{r}_{i_0}$ [1]:

$$\langle \mathbf{R}_{\mathcal{I}} - \mathbf{r}_{i_0}\rangle = \langle \mathbf{R}_{\mathcal{I}}\rangle - \mathbf{r}_{i_0} \approx \overline{\mathbf{U}}^* t, \tag{3.8}$$

with angular brackets defined below in Eq. (3.10). Similarly calculation of the dispersivity dyadic $\overline{\mathbf{D}}^*$ follows from

knowledge of the mean-squared vector displacement of the Brownian particle from its mean position $\langle \mathbf{R}_{\mathcal{I}} \rangle$ at time t [1]:

$$\langle [\mathbf{R}_{\mathcal{I}} - \langle \mathbf{R}_{\mathbf{I}} \rangle][\mathbf{R}_{\mathcal{I}} - \langle \mathbf{R}_{\mathcal{I}} \rangle] \rangle \approx 2\overline{\mathbf{D}}^* t. \tag{3.9}$$

The average values appearing in these expressions represent summations over the global graph

$$\langle \mathbf{R}_{\mathcal{I}} \rangle = \sum_{\Gamma_g} (\mathbf{R}_{\mathbf{I}} + \mathbf{r}_i) P(\mathbf{I}, i, t | i_0). \tag{3.10}$$

Since the decay of the transient solution of Eq. (3.4) is exponential in time [1], the average values defined above become asymptotically independent of i_0 (and, equivalently, $\mathbf{r}_{i_0}$). This tendency of the particle to lose ''memory'' of the position i_0 of its initial local (vertex) introduction into the network proves fundamental in the asymptotic theory to follow (cf. Sec. V A).

IV. MOMENT-MATCHING SCHEME

Calculation of the macrotransport parameters $\overline{\mathbf{U}}^*$ and $\overline{\mathbf{D}}^*$ from the present network model derives via a Taylor-Aris-like moment-matching scheme for the asymptotic global moments of the probability density, as detailed in Sec. V. As a prelude to this, we invoke the generic scheme employed by Adler and Brenner [14] to calculate these moments prior to effecting their asymptotic expansions, including appropriate modifications allowing for the incorporation of molecular diffusion effects into the analysis.

A. Local moments

Define the mth-local moment ($m = 0, 1, 2, \ldots$) of the conditional probability density as the m-adic [59],

$$\mathbf{P}_m(i, t | t_0) \overset{\text{def.}}{=} \sum_{\mathbf{I}} (\mathbf{R}_{\mathbf{I}})^m P(\mathbf{I}, \ i, \ t | i_0), \tag{4.1}$$

the indicated summation being defined as the triple sum over all unit-cell indices

$$\sum_{\mathbf{I}} \overset{\text{def.}}{=} \sum_{I_1=-\infty}^{\infty} \sum_{I_2=-\infty}^{\infty} \sum_{I_3=-\infty}^{\infty}. \tag{4.2}$$

The differential equation governing $\mathbf{P}_m$ is formed by multiplying the node conservation equation (3.4) by the quantity $(\mathbf{R}_{\mathbf{I}})^m \equiv \mathbf{R}_{\mathbf{I}}\mathbf{R}_{\mathbf{I}} \cdots \mathbf{R}_{\mathbf{I}}$ (m times), and subsequently performing the triple summation (4.2), thereby furnishing the following ordinary differential equation for $\mathbf{P}_m(i, t | i_0)$:

$$\begin{aligned} v(i) \frac{d\mathbf{P}_m(i, t | i_0)}{dt} &= \delta(i, i_0)\delta(t)\delta(m, 0) + \sum_{\substack{j \in \Omega^+(i) \\ j = \{i', i\}}} [c(j) + d(j)] \\ &\times \left[\sum_{\mathbf{I}} (\mathbf{R}_{\mathbf{I}})^m P(\mathbf{I}', \ i', \ t | i_0) \right] - \sum_{\substack{j \in \Omega^+(i) \\ j = \{i', i\}}} d(j) \mathbf{P}_m(i, t | i_0) \\ &- \sum_{\substack{j \in \Omega^-(i) \\ j = \{i, i'\}}} [c(j) + d(j)] \mathbf{P}_m(i, t | i_0) \\ &+ \sum_{\substack{j \in \Omega^-(i) \\ j = \{i, i'\}}} d(j) \left[\sum_{\mathbf{I}} (\mathbf{R}_{\mathbf{I}})^m P(\mathbf{I}', \ i', \ t | i_0) \right], \end{aligned} \tag{4.3}$$

where $\delta(m, 0)$ is the Kronecker delta function. Whereas the ordinary differential equation governing the evolution of P itself on the global graph requires detailed information regarding the behavior of P throughout the entire infinite network, the solution of the governing equations for $\mathbf{P}_m$ is contained wholly within the local graph Γ_l.

Evaluation of sums involving terms of the type $(\mathbf{R}_{\mathbf{I}})^m P(\mathbf{I}', i', t | i_0)$ appearing in Eq. (4.3) may be effected by adding and subtracting $\mathbf{R}_{\mathbf{I}'}$, as follows [14]:

$$\mathbf{R}_{\mathbf{I}} = (\mathbf{R}_{\mathbf{I}} - \mathbf{R}_{\mathbf{I}'}) + \mathbf{R}_{\mathbf{I}'} = \mathbf{R}(j) + \mathbf{R}_{\mathbf{I}'}, \tag{4.4}$$

whereupon the first few moments are found to obey the following sequence of recurrence relations:

$$\begin{aligned} v(i) \frac{dP_0(i, \ t | i_0)}{dt} &= \delta(i, i_0)\delta(t) + \sum_{\substack{j \in \Omega^+(i) \\ j = \{i', i\}}} c(j) P_0(i', \ t | i_0) + d(j)[P_0(i', \ t | i_0) - P_0(i, \ t | i_0)] \\ &- \sum_{\substack{j \in \Omega^-(i) \\ j = \{i, i'\}}} c(j) P_0(i, \ t | i_0) + d(j)[P_0(i, \ t | i_0) - P_0(i', \ t | i_0)], \end{aligned} \tag{4.5}$$

$$\begin{aligned} v(i) \frac{d\mathbf{P}_1(i, \ t | i_0)}{dt} &= \sum_{\substack{j \in \Omega^+(i) \\ j = \{i', i)\}}} c(j)[\mathbf{R}(j) P_0(i', \ t | i_0) + \mathbf{P}_1(i', \ t | i_0)] - \sum_{\substack{j \in \Omega^-(i) \\ j = \{i, i'\}}} c(j) \mathbf{P}_1(i, t | i_0) + \sum_{\substack{j \in \Omega^+(i) \\ j = \{i', i\}}} d(j)[\mathbf{R}(j) P_0(i', \ t | i_0) \\ &+ \mathbf{P}_1(i', \ t | i_0) - \mathbf{P}_1(i, \ t | i_0] - \sum_{\substack{j \in \Omega^-(i) \\ j = \{i, i'\}}} d(j)[\mathbf{P}_1(i, \ t | i_0) + \mathbf{P}_1(i', \ t | i_0) + \mathbf{R}(j) P_0(i', \ t | i_0)], \end{aligned} \tag{4.6}$$

$$v(i)\frac{d\mathbf{P}_2(i,\ t|i_0)}{dt}=\sum_{\substack{j\in\Omega^+(i)\\ j=\{i',i\}}}c(j)\begin{bmatrix}\mathbf{R}(j)\mathbf{R}(j)P_0(i',\ t|i_0)+\mathbf{R}(j)\mathbf{P}_1(i',\ t|i_0)\\ +\mathbf{P}_1(i',\ t|i_0)\mathbf{R}(j)+\mathbf{P}_2(i',\ t|i_0)\end{bmatrix}-\sum_{\substack{j\in\Omega^-(i)\\ j=\{i,i'\}}}c(j)\mathbf{P}_2(i,t|i_0)$$
$$+\sum_{\substack{j\in\Omega^+(i)\\ j=\{i',i\}}}d(j)\begin{bmatrix}\mathbf{R}(j)\mathbf{R}(j)P_0(i',\ t|i_0)+\mathbf{R}(j)\mathbf{P}_1(i',\ t|i_0)\\ +\mathbf{P}_1(i',\ t|i_0)\mathbf{R}(j)+\mathbf{P}_2(i',\ t|i_0)-\mathbf{P}_2(i,\ t|i_0)\end{bmatrix}$$
$$-\sum_{\substack{j\in\Omega^-(i)\\ j=\{i,i'\}}}d(j)\begin{bmatrix}\mathbf{P}_2(i,\ t|i_0)-\mathbf{R}(j)\mathbf{R}(j)P_0(i',\ t|i_0)\\ +\mathbf{R}(j)\mathbf{P}_1(i',\ t|i_0)+\mathbf{P}_1(i',\ t|i_0)\mathbf{R}(j)-\mathbf{P}_2(i',\ t|i_0)\end{bmatrix}. \tag{4.7}$$

The appearance of the macroscopic jump vector in the summations over $j\in\Omega^-(i)$ in Eqs. (4.6)–(4.7) necessitates using $-\mathbf{R}(j)$, rather than $\mathbf{R}(j)$, owing to the fact that the macroscopic jump vector was previously defined in Eq. (2.2) for edges *entering* the unit cell, whereas that in $j\in\Omega^-(i)$ involves edges *exiting* the unit cell. It is trivial to show that the macroscopic jump vector for an edge exiting the unit cell is equal in magnitude and opposite in direction to that for a homologous edge entering the unit cell; hence, the change in algebraic sign. The latter issue, solely a by-product of incorporating molecular diffusion into our model, did not arise in the prior, exclusively convective, solute transport model of Adler and Brenner [14].

With the continued presence of the unit impulse, appearing in the differential equation for the zeroth-order moment (4.5), the conservation principle embodied in Eq. (3.1) for the global graph adopts the form

$$\sum_{i\in V\Gamma_l}v(i)P_0(i,t|i_0)=1\quad(t>0), \tag{4.8}$$

reflecting the unitary probability that the particle is located for all times after its introduction into the network within some unit-cell subvolume element. In contrast, higher-order local moments are not similarly ''conserved,'' but rather grow in time.

B. Global moments

Define the mth-global moment $(m=0,1,2,...)$ as the m-adic,

$$\mathbf{M}_m(t|i_0)\overset{\text{def.}}{=}\sum_{i\in V\Gamma_l}v(i)\mathbf{P}_m(i,\ t|i_0). \tag{4.9}$$

In performing summations over the local graph, it is useful to note that for a given nodal quantity $\phi(i)$ and edge quantity $\epsilon(j)$, the strong connectivity of the graph furnishes the identity

$$\sum_{\substack{j\in E\Gamma_l\\ j\in\Omega^+}}\epsilon(j)\phi(i')=\sum_{\substack{j\in E\Gamma_l\\ j\in\Omega^-}}\epsilon(j)\phi(i). \tag{4.10}$$

In expressing the latter, we have made use of the compact summation notation,

$$\sum_{\substack{j\in E\Gamma_l\\ j\in\Omega^+}}\overset{\text{def.}}{=}\sum_{i\in V\Gamma_l}\sum_{\substack{j\in\Omega^+(i)\\ j=\{i',i\}}},\qquad\sum_{\substack{j\in E\Gamma_l\\ j\in\Omega^-}}\overset{\text{def.}}{=}\sum_{i\in V\Gamma_l}\sum_{\substack{j\in\Omega^-(i)\\ j=\{i,i'\}}}. \tag{4.11}$$

To arrive at the differential equations governing the global moments, differentiate Eq. (4.9) with respect to time and substitute the resulting expression into the appropriate local moment from Eqs. (4.5)–(4.7), using the identity (4.10). For the zeroth-order moment, this procedure yields

$$\frac{dM_0}{dt}=\delta(t). \tag{4.12}$$

The latter relation expresses the conservation of total probability principle (3.1), which is directly verified by integrating Eq. (4.12) to obtain

$$M_0=\begin{cases}0 & (t\leqslant 0),\\ 1 & (t>0),\end{cases} \tag{4.13}$$

independently of i_0.

As regards higher-order moments, the first- and second-order global moments obey the respective equations

$$\frac{d\mathbf{M}_1(t|i_0)}{dt}=\sum_{\substack{j\in E\Gamma_l\\ j\in\Omega^+}}[c(j)+d(j)]\mathbf{R}(j)P_0(i',\ t|i_0)-\sum_{\substack{j\in E\Gamma l\\ j\in\Omega^-}}d(j)\mathbf{R}(j)P_0(i,\ t|i_0), \tag{4.14}$$

$$\frac{d\mathbf{M}_2(t|i_0)}{dt}=\sum_{\substack{j\in E\Gamma_l\\ j\in\Omega^+}}[c(j)+d(j)]\begin{bmatrix}\mathbf{R}(j)\mathbf{R}(j)P_0(i',\ t|i_0)+\mathbf{R}(j)\mathbf{P}_1(i',\ t|i_0)\\ +\mathbf{P}_1(i',\ t|i_0)\mathbf{R}(j)\end{bmatrix}$$
$$+\sum_{\substack{j\in E\Gamma_l\\ j\in\Omega^-}}d(j)\begin{bmatrix}\mathbf{R}(j)\mathbf{R}(j)P_0(i',\ t|i_0)-\mathbf{R}(j)\mathbf{P}_1(i',\ t|i_0)\\ -\mathbf{P}_1(i',\ t|i_0)\mathbf{R}(j)\end{bmatrix}. \tag{4.15}$$

V. ASYMPTOTIC LONG-TIME LIMITS

A. Zeroth-order moments

Asymptotic integration of the zeroth-order local moment Eq. (4.5) furnishes the long-time solution

$$P_0(i,t|i_0) \approx P_0^{\infty}(i) + \text{exp.} \tag{5.1}$$

Here and hereafter, the generic symbol ''exp'' denotes terms that are exponentially attenuated in time as $t \to \infty$. As was true of the continuous paradigm counterpart $P_0^{\infty}(\mathbf{r})$ of Eq. (5.1) [1], the time-independent probability density $P_0^{\infty}(i)$ is unconditional, whereby the probability of locating the Brownian particle at vertex i becomes independent of the initial local vertex i_0 of its introduction into the network. Substitution of Eq. (5.1) into both Eqs. (4.5) and (4.8) furnishes the following steady-state conservation equation for $P_0^{\infty}(i)$:

$$\sum_{\substack{j \in \Omega^+(i) \\ j=\{i',i\}}} c(j) P_0^{\infty}(i') + d(j)[P_0^{\infty}(i') - P_0^{\infty}(i)] - \sum_{\substack{j \in \Omega^-(i) \\ j=\{i,i'\}}} c(j) P_0^{\infty}(i) + d(j)[P_0^{\infty}(i) - P_0^{\infty}(i')] = 0, \tag{5.2}$$

supplemented by the requisite normalization condition,

$$\sum_{i \in V\Gamma_l} v(i) P_0^{\infty}(i) = 1. \tag{5.3}$$

The latter pair of equations governing $P_0^{\infty}(i)$ constitute the discrete analogs of the comparable continuous conservation equation and normalization condition governing the continuous intracellular field $P_0^{\infty}(\mathbf{r})$ arising in classical continuous macrotransport theory [1]. Moreover, in the presence of vanishing molecular diffusivity and conserved convective transport (3.6), the probability density tends towards the asymptotic value $P_0^{\infty}(i) = V^{-1}$ for all i, where $V \overset{\text{def.}}{=} \Sigma_{i \in E\Gamma_l} v(i)$ is the volume of the unit cell, in accord with the results of Adler and Brenner [14] for that case.

1. Edge transport properties in the long-time limit

The equivocal nature of the edge transport properties, which hindered a deterministic solution of the discrete ''exact'' $l \oplus L$-scale governing Eq. (3.4), vanishes in the long-time Taylor-Aris dispersion limit, $t \gg l^2/D_m$. Explicitly, satisfaction of the latter inequality assures that the Brownian particle has had the opportunity to sample *all* locations i within the unit cell numerous times, effectively achieving an equilibrium distribution $P_0^{\infty}(i)$ with respect to its local position. Since the characteristic transverse linear dimension H of a channel is assumed to be less than the length l of the unit cell (often $H \ll l$), the Brownian particle will, concomitantly, have had the opportunity to sample all channel locations within each subvolume element $v(i)$ of the cell numerous times. Consequently, achieving the asymptotic long-time limit necessitates that $t \gg H^2/D_m$, whereby the edge velocity $U(j)$ and diffusivity $D(j)$ represent *mean* l-scale solute transport properties, arising from numerous samplings of the individual channels within a cell. The latter parameters may be obtained either: (i) experimentally, using a single long channel so as to satisfy the inequality $t \gg H^2/D_m$ (where $t = l/U$ is the nominal holdup time of the particle traversing the channel of length l with mean velocity U) before the particle exits the experimental channel; or (ii) via classical macrotransport theory [1], in circumstances where hydrodynamic fluid-particle data exists.

As a further consequence of attaining this asymptotic limit, the exit channel parameter $K(j)$ constitutes the *equilibrium* distribution of edge choices. For diffusion dominated transport processes, it is our contention that the hindered-diffusion partition coefficient [60] governs the probability of the particle choosing differing intersectional egress channels, inasmuch as the partition coefficient is an equilibrium property. This coefficient may be derived rigorously, enabling systematic incorporation of a vast array of effects, including steric and electrostatic hindrances [60].

This ability to furnish formal definitions for the requisite transport parameters in a rigorous, well-defined, and experimentally realizable long-time limit renders the present discrete generalized Taylor-Aris dispersion scheme markedly less equivocal than previous network models [16–18,20,27–30,33,34] of periodically configured systems.

2. Solution for $P_0^{\infty}(i)$ in the cocycle space

In order to facilitate a formal matrix solution for the probability density, define the $n \times 1$ vector $\mathbf{P}$ whose rows are the probability densities $P_0^{\infty}(i)$. In addition, define the following pair of $m \times m$ diagonal matrices containing the effective edge transport parameters [61]:

$$\mathbf{c} = c(j)\delta(i,j), \quad \mathbf{d} = d(j)\delta(i,j), \tag{5.4}$$

where $\delta(i,j)$ is the Kronecker delta function. These definitions permit the conservation Eq. (5.2) to be represented in the compact matrix form

$$\mathbf{D} \cdot [(\mathbf{c}+\mathbf{d}) \cdot (\Pi^{(-)})^{\dagger} - \mathbf{d} \cdot (\Pi^{(+)})^{\dagger}] \cdot \mathbf{P} = \mathbf{0}, \tag{5.5}$$

with † the transposition operator. Clearly, Eq. (5.5) is satisfied by the trivial solution $\mathbf{P} = \mathbf{0}$ for the n vector elements $P_0^{\infty}(i)$, since the incidence matrix $\mathbf{D}$ is of rank $n-1$. Indeed, this rank-deficient property of the incidence matrix necessitates retaining the probability density normalization condition (3.1) in the asymptotic limit. To incorporate this normalization condition into the formal solution, define the $(n-1) \times n$ coefficient matrix $\mathbf{A}$,

$$\mathbf{A} \overset{\text{def.}}{=} \mathbf{K}^{\dagger} \cdot [(\mathbf{c}+\mathbf{d}) \cdot (\Pi^{(-)})^{\dagger} - \mathbf{d} \cdot (\Pi^{(+)})^{\dagger}], \tag{5.6}$$

as well as the $1 \times n$ vector of the nodal volumes,

$$\overset{\text{def.}}{\mathbf{v}} = v(i). \tag{5.7}$$

These permit the linearly independent, rank n matrix equation for the probability density to be expressed in the partitioned matrix form,

$$\begin{bmatrix} \mathbf{A} \\ \mathbf{v} \end{bmatrix} \cdot \mathbf{P} = \begin{bmatrix} \mathbf{0} \\ 1 \end{bmatrix}. \tag{5.8}$$

B. First-order moments

1. Mean velocity vector $\overline{U}^*$

As in classical generalized Taylor-Aris dispersion theory [1], the mean particle velocity vector may be calculated from the following asymptotic expression derived from Eqs. (3.8), (3.10), (4.1), and (4.9):

$$\overline{\mathbf{U}}^* = \lim_{t\to\infty} \frac{d\mathbf{M}_1}{dt}. \tag{5.9}$$

Substitution of Eq. (4.14) into the latter, together with use of Eqs. (4.10) and (5.1), enables $\overline{\mathbf{U}}^*$ to be calculated from knowledge of $P_0^\infty(i)$ via the following generic paradigmatic relation:

$$\overline{\mathbf{U}}^* = \sum_{\substack{j\in E\Gamma_l \\ j\in\Omega^+}} c(j)\mathbf{R}(j)P_0^\infty(i') + d(j)\mathbf{R}(j)[P_0^\infty(i') - P_0'(i)]. \tag{5.10}$$

Upon setting $d(j)=0$ and $P_0^\infty(i')=V^{-1}$, the latter agrees with the expression previously derived elsewhere [14] for the case of purely convective solute transport.

2. Derivation of the B-equation

Assume, subject to *a posteriori* verification, an asymptotic trial solution of the form

$$\mathbf{P}_1(i,\ t|i_0) \approx P_0^\infty(i)[\overline{\mathbf{U}}^* t + \mathbf{B}(i)] + \text{exp}, \tag{5.11}$$

with $\mathbf{B}(i)$ a time- and i_0-independent vector to be determined. Introduce Eqs. (5.1) and (5.11) into Eq. (4.6), subsequently canceling time-dependent terms with Eq. (5.2), so as to arrive at the following difference equation governing the vector $\mathbf{B}(i)$ at each node on the local graph:

$$\begin{aligned} &\sum_{\substack{j\in\Omega^+(i) \\ j=\{i',i\}}} c(j)P_0^\infty(i')\mathbf{B}(i') + d(j)[P_0^\infty(i')\mathbf{B}(i') - P_0^\infty(i)\mathbf{B}(i)] \\ &\quad - \sum_{\substack{j\in\Omega^-(i) \\ j=\{i,i'\}}} c(j)P_0^\infty(i)\mathbf{B}(i) \\ &\quad + d(j)[P_0^\infty(i)\mathbf{B}(i) - P_0^\infty(i')\mathbf{B}(i')] \\ &= v(i)P_0^\infty(i)\overline{\mathbf{U}}^* - \alpha(i), \end{aligned} \tag{5.12}$$

with $\alpha(i)$ the node-based vector

$$\begin{aligned} \alpha(i) = &\sum_{\substack{j\in\Omega^+(i) \\ j=\{i',i\}}} [c(j)+d(j)]\mathbf{R}(j)P_0^\infty(i') \\ &- \sum_{\substack{j\in\Omega^-(i) \\ j=\{i,i'\}}} d(j)\mathbf{R}(j)P_0^\infty(i'). \end{aligned} \tag{5.13}$$

It is readily confirmed from Eqs. (5.2) and (5.12), as was true for both continuous [1] and nondiffusive discrete [14] generalized Taylor-Aris modeling, that the $\mathbf{B}$ vector is uniquely defined only to within an arbitrary additive constant vector. Moreover, as in those earlier cases, the forcing function appearing on the RHS of Eq. (5.12) represents the difference between the mean and "local" vertex velocities. This velocity disparity furnishes the physical mechanism underlying the origin of dispersion within the network. The time- and i_0-independence of the equation governing $\mathbf{B}(i)$ observed in Eq. (5.12) furnishes *a posteriori* verification of the assumed trial solution (5.11) for $\mathbf{P}_1$. This "transport equation" for the $\mathbf{B}$ field plays a fundamental role in subsequent dispersion calculations. Its solution within the cocycle space is discussed forthwith.

Substitution of Eq. (5.11) into (4.9) (with $m=1$), together with use of Eq. (5.3), furnishes the following asymptotic form for $\mathbf{M}_1$:

$$\mathbf{M}_1(t) \approx \overline{\mathbf{U}}^* t + \overline{\mathbf{B}} + \text{exp}, \tag{5.14}$$

wherein $\overline{\mathbf{B}}$ is the time-independent constant vector

$$\overline{\mathbf{B}} = \sum_{i\in V\Gamma_l} v(i)P_0^\infty(i)\mathbf{B}(i). \tag{5.15}$$

3. Solution of the B-equation in the cocycle space

Since each of the n different $\mathbf{B}$ vectors is determined only to within a single arbitrary, additive constant, say, $\mathbf{B}(i^*)$, the $n-1$ dimensional cocycle space furnishes a systematic method for identifying the basis node i^* as that not appearing in the basis set of the cocycle space. Adapting the method of Adler and Brenner [14] to the problem at hand, define the following pair of $m\times 3$ matrices:

$$\beta^-(j) = P_0^\infty(i)[\mathbf{B}^\dagger(i) - \mathbf{B}^\dagger(i^*)] \quad [j\in\Omega^-(i)], \tag{5.16}$$

$$\beta^+(j) = P_0^\infty(i)[\mathbf{B}^\dagger(i) - \mathbf{B}^\dagger(i^*)] \quad [j\in\Omega^+(i)], \tag{5.17}$$

as well as the $(n-1)\times 3$ matrix,

$$\alpha^*(i) = [v(i)P_0^\infty(i)\overline{\mathbf{U}}^* - \alpha(i)]^\dagger \quad (i\neq i_0). \tag{5.18}$$

With use of the preceding matrix definitions, Eq. (5.12) may be recast into the compact matrix form,

$$\mathbf{K}^\dagger \cdot [(\mathbf{c}+\mathbf{d})\cdot\beta^- - \mathbf{d}\cdot\beta^+] = \alpha^*. \tag{5.19}$$

Eventual computation of the dispersivity [cf. Eq. (5.32)] necessitates use of the edge-based vector,

$$\mathbf{b}(j) \overset{\text{def.}}{=} \mathbf{B}(i) - \mathbf{B}(i') \quad (j=\{i',i\}), \tag{5.20}$$

where the edge is oriented with its initial vertex at i'. Define an $m\times 3$ matrix, $\mathbb{B}$, whose rows are the vectors $\mathbf{b}^{\dagger}(j)$, the matrix $\mathbb{B}$ being computed from the relationships [14]

$$\beta^{-}(j)=\mathcal{B}^{-}\cdot\mathbb{B}, \quad \beta^{+}(j)=\mathcal{B}^{+}\cdot\mathbb{B}, \tag{5.21}$$

where $\mathcal{B}^{-}$ and $\mathcal{B}^{+}$ are $m\times m$ matrices involving the probability density $P_0^{\infty}(i)$. Consequently, Eq. (5.19) may be rewritten as

$$\mathbf{K}^{\dagger}\cdot[(\mathbf{c}+\mathbf{d})\cdot\mathcal{B}^{-}-\mathbf{d}\cdot\mathcal{B}^{+}]\cdot\mathbb{B}=\alpha^{*}. \tag{5.22}$$

Although the $(n-1)\times m$ coefficient matrix $\mathbf{K}^{\dagger}\cdot[(\mathbf{c}+\mathbf{d})\cdot\mathcal{B}^{-}-\mathbf{d}\cdot\mathcal{B}^{+}]$ is not square, it is always possible to augment the coefficient matrix with additional rows containing the null sum of $\mathbf{b}(j)$ vectors along a cycle of the graph [52], with concomitant rows of zeros in the solution vector α^{*}.

C. Second-order moments

Substitute the asymptotic solutions (5.1) and (5.11) into Eq. (4.15), making use of Eq. (5.10), so as to arrive at the following asymptotic expression for the second-order global moment:

$$\begin{aligned}\frac{d\mathbf{M}_2(t)}{dt} \approx{}& 2\overline{\mathbf{U}}^{*}\overline{\mathbf{U}}^{*}t+\sum_{\substack{j\in E\Gamma_l\\ j\in\Omega^{+}}}[c(j)+d(j)]P_0^{\infty}(i')\\ &\times[\mathbf{R}(j)\mathbf{R}(j)+\mathbf{R}(j)\mathbf{B}(i')+\mathbf{B}(i')\mathbf{R}(j)]\\ &+\sum_{\substack{j\in E\Gamma_l\\ j\in\Omega^{-}}} d(j)P_0^{\infty}(i')[\mathbf{R}(j)\mathbf{R}(j)-\mathbf{R}(j)\mathbf{B}(i')\\ &-\mathbf{B}(i')\mathbf{R}(j)]+\text{exp.}\end{aligned} \tag{5.23}$$

The dispersivity dyadic may be computed from the following expression [1], derived from Eqs. (3.9), (3.10), (4.1), and (4.9):

$$\overline{\mathbf{D}}^{*}=\frac{1}{2}\lim_{t\to\infty}\frac{1}{2}(\mathbf{M}_2-\mathbf{M}_1\mathbf{M}_1). \tag{5.24}$$

The RHS of the latter may be evaluated by use of Eqs. (5.10), (5.14), (5.15), and (5.23), together with use of the definition of the $\mathbf{b}(j)$ vector (5.20) and Eq. (4.10), to eventually furnish the formula

$$\begin{aligned}\overline{\mathbf{D}}^{*}={}&\text{sym}\sum_{\substack{j\in E\Gamma_l\\ j\in\Omega^{+}}}\{c(j)P_0^{\infty}(i')+d(j)[P_0^{\infty}(i')+P_0^{\infty}(i)]\}\\ &\times[\tfrac{1}{2}\mathbf{R}(j)\mathbf{R}(j)-\mathbf{R}(j)\mathbf{b}(j)]+\text{sym}(\mathbf{E}),\end{aligned} \tag{5.25}$$

with $\mathbf{E}$ the tensor

$$\mathbf{E}=\sum_{i\in V\Gamma_l}[\alpha(i)\mathbf{B}(i)-v(i)P_0^{\infty}(i)\overline{\mathbf{U}}^{*}\mathbf{B}(i)]. \tag{5.26}$$

Notationally, the symmetry operator for a generic matrix $\mathbf{XY}$ is defined by the expression

$$\text{sym}(\mathbf{XY}) \overset{\text{def.}}{=} \tfrac{1}{2}(\mathbf{XY}+\mathbf{YX}). \tag{5.27}$$

Evaluation of $\overline{\mathbf{D}}^{*}$ via Eq. (5.25) requires knowledge of $\mathbf{B}(i)$ [as well as of $P_0^{\infty}(i)$].

Additional computational simplifications of Eq. (5.25) are readily effected. Similar to Adler and Brenner [14], we identify the terms appearing in the summation (5.26) for $\mathbf{E}$ as being the negative of the RHS of Eq. (5.12) multiplied by $\mathbf{B}(i)$. Consequently, the expression for $\mathbf{E}$ may be reformulated upon multiplying Eq. (5.12) by $\mathbf{B}(i)$, summing over $i\in V\Gamma_l$, and using Eqs. (4.10) and (5.20), so as to eventually obtain

$$\begin{aligned}\mathbf{E}={}&\sum_{\substack{j\in E\Gamma_l\\ j\in\Omega^{+}}} d(j)P_0^{\infty}(i)\mathbf{B}(i)\mathbf{b}(j)\\ &-[c(j)+d(j)]P_0^{\infty}(i')\mathbf{B}(i')\mathbf{b}(j).\end{aligned} \tag{5.28}$$

To effect further simplifications, multiply Eq. (5.2) by $\mathbf{B}(i)\mathbf{B}(i)$, and sum over $i\in V\Gamma_l$, using Eq. (4.10), to obtain

$$\begin{aligned}&\sum_{\substack{j\in E\Gamma_l\\ j\in\Omega^{+}}}\{[c(j)+d(j)]P_0^{\infty}(i')-d(j)P_0^{\infty}(i)\}\\ &\quad\times[\mathbf{B}(i)\mathbf{B}(i)-\mathbf{B}(i')\mathbf{B}(i')]=\mathbf{0}.\end{aligned} \tag{5.29}$$

Writing twice the symmetric part of $\mathbf{E}$ using Eq. (5.28), and adding Eq. (5.29), finally yields

$$\begin{aligned}2\,\text{sym}(\mathbf{E})={}&\sum_{\substack{j\in E\Gamma_l\\ j\in\Omega^{+}}}\{c(j)P_0^{\infty}(i')\\ &+d(j)[P_0^{\infty}(i')+P_0^{\infty}(i)]\}\mathbf{b}(j)\mathbf{b}(j).\end{aligned} \tag{5.30}$$

To arrive at a canonical form for ultimately calculating the dispersivity dyadic, define the edge-based vector,

$$\tilde{\mathbf{b}}(j) \overset{\text{def.}}{=} \mathbf{R}(j)-\mathbf{b}(j), \tag{5.31}$$

and substitute Eq. (5.30) into Eq. (5.25), thereby obtaining

$$\overline{\mathbf{D}}^{*}=\tfrac{1}{2}\sum_{\substack{j\in E\Gamma_l\\ j\in\Omega^{+}}}\{c(j)P_0^{\infty}(i')+d(j)[P_0^{\infty}(i')+P_0^{\infty}(i)]\}\tilde{\mathbf{b}}(j)\tilde{\mathbf{b}}(j). \tag{5.32}$$

The preceding generic dispersivity formula properly reduces to the prior result of Adler and Brenner [14] upon setting $d(j)=0$ and $P_0^{\infty}(i)=V^{-1}$. Equation (5.32) represents the fundamental paradigm whereby $\overline{\mathbf{D}}^{*}$ can be calculated from the prescribed discrete l-scale data.

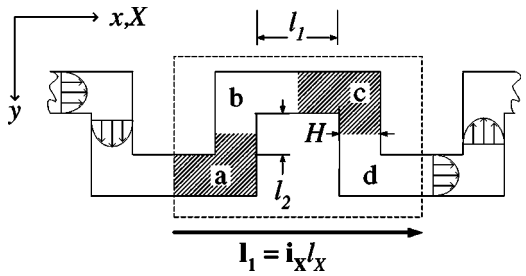

FIG. 4. Rectangular serpentine channel comprised of infinitely extended parallel plates of constant channel width H (and area A, $A/H^2 \gg 1$). Channels oriented locally in the x and y direction are, respectively, of lengths l_1 and l_2. The unit cell of length l_X in the X direction is indicated by the dashed box, with the periodicity and net particle transport processes occurring solely in the direction of the unit vector **x**. Alternating shaded/unshaded regions correspond to the nodes in the local graph of Fig. 5.

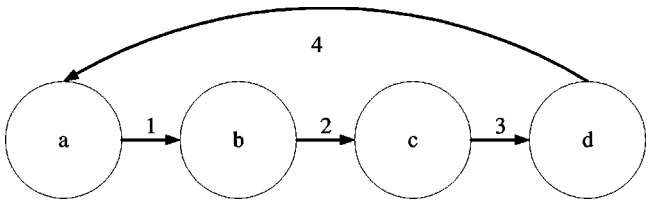

FIG. 5. Local graph for the serpentine channel. The convective transport coefficient for all edges is equal to the volumetric fluid flow rate $c=Q$. Edges 1 and 3 are oriented in the y direction with diffusive transport coefficient $d_y=DA/l_2$, whereas edges 2 and 4 are oriented in the x direction with diffusive transport coefficient $d_x=DA/l_1$.

VI. DISCUSSION

A. Dispersion in serpentine microchannels

By way of presenting an ''elementary,'' independently confirmable, illustrative example, the present subsection furnishes an explicit network theory calculation of the mean velocity and dispersivity accompanying pressure-driven flow occurring in a serpentine microchannel, as depicted in Fig. 4. Such devices, currently proposed for compact chromatographic separations on microchips [62], have been analyzed elsewhere [63] within the framework of classical continuous Taylor-Aris dispersion theory for spatially periodic systems.

The network is chosen to consist of a rectangular collocation of channels of constant cross-sectional width H (and area A, $A/H^2 \gg 1$), arranged with period l_X in the global X direction ($-\infty < X < \infty$). Channels oriented locally within the unit cell in the x and y directions possess lengths l_1 and l_2, respectively, with all channel intersections possessing equal volume. The total volume V of the unit cell accessible to the particle is written as the product of the channel area A and a characteristic linear (arc length) dimension l_s.

Particle transport is animated by imposing a uniform macroscopic axial pressure gradient upon the interstitial fluid, giving rise to a mean solvent (and hence entrained solute particle) velocity $\overline{v}$ within the individual channels. The dispersed particles, entrained in the solvent flow, are assumed to be pointsize in comparison with the channel cross-sectional width, whereupon no hydrodynamic wall effects arise in the subsequent calculations. Consequently, the molecular diffusivity of the particles in the channels is taken to be the constant scalar value D_m. Since the *net* particle (and fluid) transport is necessarily unidirectional, taking place in the X direction, scalar notation will be employed in what follows, with the tacit understanding that all vectors and dyadics appearing within the general theory are directed along the X axis.

Figure 5 depicts the local graph derived from the ''continuous'' portrayal in Fig. 4. Each node consists of one half the volume of both an x- and y-directed channel, together with an intersection, so that the nodal volumes are all equal: $v(i)=V/4$ for all i. The geometry of the serpentine configuration is captured by the following incidence matrix, cocycle matrix, and macroscopic jump vector for the local graph:

$$\mathbf{D}=\begin{bmatrix} -1 & 0 & 0 & 1 \\ 1 & -1 & 0 & 0 \\ 0 & 1 & -1 & 0 \\ 0 & 0 & 1 & -1 \end{bmatrix},$$

$$\mathbf{K}=\begin{bmatrix} -1 & 1 & 0 \\ 0 & -1 & 1 \\ 0 & 0 & -1 \\ 1 & 0 & 0 \end{bmatrix}, \quad \mathbf{R}=\begin{pmatrix} 0 \\ 0 \\ 0 \\ l_X \end{pmatrix}. \tag{6.1}$$

The mean velocity $\overline{v}$ in the channels specifies the edge convection parameter, $c(j)=Q=\overline{v}A$ for all j, and edge diffusivities, $d(1)=d(3)=d_y$ and $d(2)=d(4)=d_x$, wherein,

$$d_x=\frac{DA}{l_1}, \quad d_y=\frac{DA}{l_2}, \tag{6.2}$$

with D the channel-scale Taylor-Aris dispersivity prevailing within the pair of channel types. For a bounded, parallel-plate configuration of effectively infinite aspect ratio ($A/H^2 \gg 1$), the channel-scale dispersivity possesses the form [64,65]

$$D=D_m+\frac{1}{210}\frac{(\overline{v}H)^2}{D_m}f\left(\frac{A}{H^2}\right), \tag{6.3}$$

with $f(A/H^2)=7.951$ in the large aspect ratio limit.

The governing matrix equation for the $P_0^\infty(i)$ appearing in Eq. (5.8) is of the form

$$\begin{bmatrix} -\sigma & d_y & 0 & Q+d_x \\ Q+d_y & -\sigma & d_x & 0 \\ 0 & Q+d_x & -\sigma & d_y \\ V/4 & V/4 & V/4 & V/4 \end{bmatrix}\begin{bmatrix} P_0^\infty(a) \\ P_0^\infty(b) \\ P_0^\infty(c) \\ P_0^\infty(d) \end{bmatrix}=\begin{bmatrix} 0 \\ 0 \\ 0 \\ 1 \end{bmatrix}, \tag{6.4}$$

with σ the parameter

$$\sigma=Q+d_x+d_y. \tag{6.5}$$

Clearly, Eq. (6.4) possesses the solution $P_0^{\infty}(i)=V^{-1}$ for all i. Substitution into Eq. (5.10) furnishes the L-scale mean velocity through the serial sequence of serpentine channels

$$\overline{U}^{*}=\tau_X\overline{v}, \tag{6.6}$$

where the dimensionless parameter $\tau_X=l_X/l_s$ represents the ''tortuosity'' l_s of the channel projected onto the X axis, the direction of net solute (and solvent) transport. The mean velocity $\overline{U}^{*}$ given by Eq. (6.6) is identical to that obtained alternatively via continuous Taylor dispersion theory [63], as well as from intuitive arguments based upon the nominal holdup time of the solvent (and hence, of the particle) as the fluid traverses a serpentine unit cell.

The structure of the cocycle matrix identifies $B(i^{*})=B(d)$. Consequently, Eq. (5.19) possesses the explicit form

$$\begin{bmatrix} -\sigma & d_y & 0 \\ Q+d_y & -\sigma & d_x \\ 0 & Q+d_x & -\sigma \end{bmatrix}\begin{bmatrix} B(a)-B(d) \\ B(b)-B(d) \\ B(c)-B(d) \end{bmatrix}=\begin{bmatrix} \frac{3}{4}Ql_X-d_xl_X \\ \frac{1}{4}Ql_X \\ \frac{1}{4}Ql_X \end{bmatrix}, \tag{6.7}$$

whose solution, in terms of the β^{-} vector, is

$$\beta^{-}(j)=\frac{l_X}{4V}\begin{bmatrix} \dfrac{2Dl_2+3\overline{v}l_1l_2+2Dl_1}{D(l_1+l_2)+\overline{v}l_1l_2} \\ 2 \\ \dfrac{l_2(\overline{v}l_1+2D)}{D(l_1+l_2)+\overline{v}l_1l_2} \\ 0 \end{bmatrix}. \tag{6.8}$$

Conversion to $\mathbb{B}$ via Eq. (5.20) is accomplished by means of the transformation matrix

$$\mathcal{B}^{-}=(P_0^{\infty})^{-1}\begin{bmatrix} -1 & 1 & 0 & 0 \\ 0 & -1 & 1 & 0 \\ 0 & 0 & -1 & 0 \\ 1 & 0 & 0 & 0 \end{bmatrix}. \tag{6.9}$$

After transforming to $\tilde{b}$ via Eq. (5.31), application of Eq. (5.32) furnishes the dispersivity,

$$\frac{\overline{D}^{*}}{D}=\frac{\tau_X^2}{8}\left[\frac{4+2\tau_1\tau_2\mathrm{Pe}_T+\tau_1\tau_2\mathrm{Pe}_T^2}{\tau_1+\tau_2+\tau_1\tau_2\mathrm{Pe}_T}\right], \tag{6.10}$$

wherein the following dimensionless parameters appear:

$$\mathrm{Pe}_T\overset{\text{def.}}{=}\frac{\overline{v}l_s}{D}, \tag{6.11}$$

$\tau_1=l_1/l_s$, and $\tau_2=l_2/l_s$. The latter pair represent the channel contributions to the tortuosity. The parameter Pe_T has been referred to elsewhere as the Taylor [33] or macroscale-[17] Péclet number.

The limiting behavior displayed by Eq. (6.10) in the respective cases $\mathrm{Pe}_T\ll 1$ and $\mathrm{Pe}_T\gg 1$ accords with results obtained previously via classical continuous theories. Thus, Rush *et al.* [63] examined the dispersion occurring in (intersection-free) serpentine microchannels in the limit of two-dimensional parabolic Poiseuille flow everywhere within the network, corresponding here to the limits $l_1\to l_X/2$, $l_2\to(l_s-l_X)/2$, and $\mathrm{Pe}_T\to 0$. The vanishingly small Péclet number in this limit implies a diffusion dominated process, where the ensuing rapid diffusive mixing renders the graph-theoretical description of the transport process essentially indistinguishable from the exact continuous description. In this limit,

$$\overline{D}^{*}=\tau_X^2D, \tag{6.12}$$

in accord with prior conclusions [63], as well as with existing formulas for the effective molecular diffusivity occurring in tortuous porous media in the strict nonconvective limit, $\overline{v}\to 0$ [31].

In the opposite, infinite Taylor-Péclet number limit, $\mathrm{Pe}_T\to\infty$, Eq. (6.10) reduces to

$$\frac{\overline{D}^{*}}{D_m}=\left(\frac{\tau_Xl_s}{8H}\right)\mathrm{Pe}=\left(\frac{l_X}{8H}\right)\mathrm{Pe}, \tag{6.13}$$

with Pe the Péclet number, based upon the molecular diffusivity,

$$\mathrm{Pe}\overset{\text{def.}}{=}\frac{\overline{v}H}{D_m}. \tag{6.14}$$

The dispersivity/molecular diffusivity ratio appearing in Eq. (6.13) scales linearly with Péclet number, with the proportionality coefficient functionally dependent upon the explicit array configuration. This conclusion accords with prevailing theories for convection-dominated or hydrodynamically dominated dispersion (''mechanical dispersion'') occurring in tortuous porous media [66,67].

B. The "simple" network

Our second and final example illustrates the usefulness of the present discrete theory in computing mean solute transport rates for a ''simple'' network. By ''simple'' is meant that only one intersection (albeit, perhaps, of multiple channels) is present within the repetitive unit cell. Figure 6 depicts such a network, wherein the apparent complexity of the medium serves to underscore potential difficulties that would be encountered in the application of continuous Taylor-Aris dispersion theory. Numerous microfluidic devices exist whose geometries are adequately captured by this simple network model, including both micropatterned vector chromatography chips [3,4] and entropic trapping devices [9]. Explicitly, the vector chromatography chips produced by Austin and co-workers [3,4] are comprised of a rectangular array of solid (rounded) rectangular obstacles, with solute transport occurring within the solvent-filled interstices between obstacles. In effect, our prior analysis [5] of such devices is equipollent with the present simple network theory, in which the unit cell consists of but a single intersection connecting a

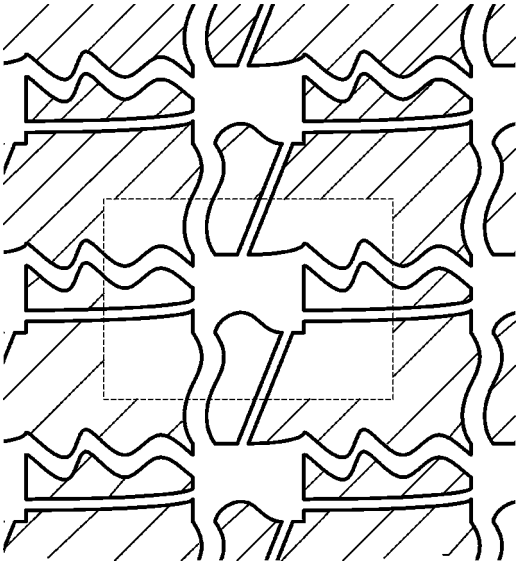

FIG. 6. Schematic of a simple network in which the repetitive unit cell, denoted by the dashed lines, consists of a number of channels exiting and entering a single intersection. Such networks result in major simplifications of the discrete Taylor-Aris dispersion analysis.

narrow channel, oriented in the y direction, to a wider channel, oriented orthogonally in the x direction.

Significant reductions in the computational scheme are immediately effected in the ''simple'' network limit. Since the unit cell is comprised of but a single intersection, the unconditional probability density assumes the form $P_0^\infty = V^{-1}$, wherein V is the total volume of the channels and intersections contained within the boundaries of the unit cell. Moreover, calculation of the dispersivity is vastly simplified by noting that $\mathbf{b}=\mathbf{0}$, owing to the fact that every edge on the local graph is a loop. Armed with the latter data, the canonical expressions (5.10) and (5.32) reduce simply to the respective forms

$$\overline{\mathbf{U}}^* = V^{-1} \sum_{\substack{j \in E\Gamma_l \\ j \in \Omega^+}} c(j)\mathbf{R}(j), \tag{6.15}$$

$$\overline{\mathbf{D}}^* = \frac{1}{2V} \sum_{\substack{j \in E\Gamma_l \\ j \in \Omega^+}} [c(j)+2d(j)]\mathbf{R}(j)\mathbf{R}(j). \tag{6.16}$$

The latter pair of formulas render transparent several fundamental properties of the simple network. The $\mathcal{I}$-space uniformity of the network reduces the mean velocity vector to a sum of purely convective contributions. In the network-level description of the periodic geometry, diffusive contributions to the mean velocity arise from nodal differences in probability density, rather than any finer-scale **R**-space gradients—the former vanishing within the single-node simple network. Rather, the diffusional transport processes occurring in the network description are manifested in the dispersivity dyadic. As is readily identified via Eq. (6.16), dispersion within the simple network arises from two fundamental sources: (i) a contribution $d(j)\mathbf{R}(j)\mathbf{R}(j)$, representing dispersive processes occurring within the channels; and (ii) a contribution $c(j)\mathbf{R}(j)\mathbf{R}(j)$, representing the mechanical dispersion caused by the random residence times spent by a particle within the channel intersection domain before exiting the latter and entering an abutting channel.

These simple network results furnish significant insights into the mean solute transport and dispersion rates arising in such media, as evidenced in our separate contribution [5]. As such, they are likely to prove useful in subsequent applications of our theory to the generalized Taylor-Aris dispersion phenomena occurring on chip-based microfluidic devices.

VII. CONCLUDING REMARKS

While the present discrete development is predicated upon the same rigorous method-of-moments homogenization scheme as is employed in continuous generalized Taylor-Aris dispersion theory when applied to spatially periodic media [1,36], our analysis has demonstrated the greater tractability of discrete network theory over its continuous counterpart [1] (the former approach being, albeit, more approximate). In the continuous theory, both the array geometry and interstitial transport physics are presumed to be known *exactly*, thereby rendering the computed macrotransport parameters $\overline{\mathbf{U}}^*$ and $\overline{\mathbf{D}}^*$ physically accurate and mathematically rigorous, at least in an asymptotic sense. Such rigor comes, however, at the expense of requiring the solution of two steady-state convection-diffusion(-reaction) partial differential equations for the continuous macrotransport fields $P_0^\infty(\mathbf{r})$ and $\mathbf{B}(\mathbf{r})$ at all interstitial unit-cell points $\mathbf{r}$ [1], as well as demanding precise and explicit knowledge of the phenomenological coefficients quantifying the l-scale interstitial transport processes. With the exception of but a few limiting cases, such phenomenological data are generally unavailable in the literature; even when such data are available, or calculable in principle for simple bodies such as rigid spheres, an accurate quantification of the interstitial transport physics is often nonexistent for deformable bodies (e.g., freely-draining DNA or polymer molecules). Moreover, the structure of the governing equations renders such equations insoluble in closed form for all but the most trivial of array geometries—even the simple network discussed previously [5]. Furthermore, the continuous theory's requisite unit-cell quadratures cannot generally be effected in closed form [2], even for those rare circumstances for which closed-form solutions exist for the macrotransport fields $P_0^\infty(\mathbf{r})$ and $\mathbf{B}(\mathbf{r})$ themselves appearing in the integrands of the requisite integrals.

The comments of the preceding paragraph point out that the resources required to extract useful macroscale information from the continuous microscale theory diminish the utility of such an approach, owing not only to the unavailability of pertinent transport data, but equally to the computational effort required and concomitant errors introduced via numerical discretization of the local-scale transport parameters. Indeed, in the latter context, similarities existing between finite-difference methods for solving partial differential equations and network models have been recognized for at least 30 years [68], inasmuch as the desired degree of accu-

racy inherent in any finite-difference scheme necessitates a lumped parameter approach on the scale of the discretization. Of course, the tractability of the discrete scheme presented here arises as a consequence of the *a priori* homogenization of the exact local-scale transport into the lumped-parameter edge transport coefficients $U(j)$, $D(j)$, and $K(j)$. While asymptotic definitions exist for the latter parameters under certain limiting circumstances, one cannot hope to rigorously retain the full extent of the true local-scale transport description—in particular, the complex geometry of even a well-defined, spatially periodic model porous medium. Nevertheless, the counterbalance existing between comparable approximations necessary for either a continuous or discrete model render the latter attractive for the characterization of macromolecular transport in microfluidic devices.

ACKNOWLEDGMENTS

We are grateful to Dr. Sangtae Kim of Eli Lilly and Company for his interest and encouragement in our analysis of microfluidic devices, and to James R. Bielenberg of MIT for his comments on earlier versions of this manuscript.

[1] H. Brenner and D. A. Edwards, *Macrotransport Processes* (Butterworth-Heinemann, Boston, 1993).
[2] K. D. Dorfman and H. Brenner, J. Colloid Interface Sci. **238**, 390 (2001).
[3] C. F. Chou *et al.*, Proc. Natl. Acad. Sci. U.S.A. **96**, 13762 (1999).
[4] C. F. Chou *et al.*, Electrophoresis **21**, 81 (2000).
[5] K. D. Dorfman and H. Brenner, Phys. Rev. Lett. (to be published).
[6] T. A. J. Duke and R. H. Austin, Phys. Rev. Lett. **80**, 1552 (1998).
[7] D. Ertas, Phys. Rev. Lett. **80**, 1548 (1998).
[8] P. S. Doyle and J. L. Viovy (unpublished).
[9] J. Han and H. G. Craighead, Science **288**, 1026 (2000).
[10] I. Fatt, Trans. AIME **207**, 160 (1956).
[11] P. Saffman, J. Fluid Mech. **6**, 321 (1959).
[12] J. Koplik, J. Fluid Mech. **119**, 219 (1982).
[13] P. M. Adler and H. Brenner, PCH, PhysicoChem. Hydrodyn. **5**, 245 (1984).
[14] P. M. Adler and H. Brenner, PCH, PhysicoChem. Hydrodyn. **5**, 269 (1984); P. M. Adler, *Porous Media: Geometry and Transports* (Butterworth-Heinemann, Boston, 1992).
[15] P. M. Adler and H. Brenner, PCH, PhysicoChem. Hydrodyn. **5**, 287 (1984).
[16] L. de Arcangelis, J. Koplik, S. Redner, and D. Wilkinson, Phys. Rev. Lett. **57**, 996 (1986).
[17] J. Koplik, S. Redner, and D. Wilkinson, Phys. Rev. A **37**, 2619 (1988).
[18] M. Sahimi and V. L. Jue, Phys. Rev. Lett. **62**, 629 (1989).
[19] B. E. Aviles and M. D. Levan, Chem. Eng. Sci. **46**, 1935 (1991).
[20] M. Sahimi, J. Chem. Phys. **96**, 4718 (1992).
[21] P. M. Adler, Int. J. Multiphase Flow **11**, 213 (1985).
[22] P. M. Adler, Int. J. Multiphase Flow **11**, 241 (1985).
[23] P. M. Adler, Int. J. Multiphase Flow **11**, 853 (1985).
[24] S. D. Rege and H. S. Fogler, AIChE J. **34**, 1761 (1988).
[25] A. O. Imdakm and M. Sahimi, Chem. Eng. Sci. **46**, 1977 (1991).
[26] B. Berkowitz and R. P. Ewing, Surv. Geophys. **19**, 23 (1998).
[27] C. Bruderer and Y. Bernabe, Water Resour. Res. **37**, 897 (2001).
[28] C. McGreavy, J. S. Andrade, Jr., and K. Rajagopal, Chromatographia **30**, 639 (1990).
[29] J. S. Andrade, Jr., K. Rajagopal, and C. McGreavy, Chromatographia **32**, 345 (1992).
[30] J. J. Meyers and A. I. Liapis, J. Chromatogr. A **827**, 197 (1998).
[31] J. van Brakel, Powder Technol. **11**, 205 (1975).
[32] M. Sahimi, H. T. Davis, and L. E. Scriven, Chem. Eng. Commun. **23**, 329 (1983).
[33] K. S. Sorbie and P. J. Clifford, Chem. Eng. Sci. **46**, 2525 (1991).
[34] L. Zhang and N. A. Seaton, Chem. Eng. Sci. **49**, 41 (1994).
[35] Such a regular, spatially periodic network theory may be employed in the modeling of ''random'' media by sampling numerous realizations of the randomly configured contents of unit cells, in the spirit of tube radii distributions employed elsewhere in capillary models of porous media (see, for example, [12]).
[36] H. Brenner, Philos. Trans. R. Soc. London, Ser. A **297**, 81 (1980).
[37] J. Happel and H. Brenner, *Low Reynolds Number Hydrodynamics* (Kluwer, Dordrecht, 1983).
[38] In the case of pressure-driven flow, the finite size of the particles results in a sterically excluded particle region, comprised of the slow-moving fluid streamline region near the wall, rendering the area-averaged mean velocity of the particle greater than that of the entraining fluid [39,40]. The latter phenomenon constitutes the dominant, first-order separation mechanism underlying (unidirectional) hydrodynamic chromatography.
[39] E. A. Dimarzio and C. M. Guttman, Macromolecules **3**, 131 (1970).
[40] H. Brenner and L. J. Gaydos, J. Colloid Interface Sci. **58**, 312 (1977).
[41] W. B. Russel, D. A. Saville, and W. R. Schowalter, *Colloidal Dispersions* (Cambridge University, Cambridge, 1989).
[42] G. I. Taylor, Proc. R. Soc. London, Ser. A **219**, 186 (1953).
[43] Z. Y. Yan, A. Acrivos, and S. Weinbaum, J. Fluid Mech. **229**, 1 (1991).
[44] J. Lee and J. Koplik, Phys. Fluids **11**, 76 (1999).
[45] Despite the ubiquitious use [17,18,20,28,29,33] of such parameters in graphical network models, the work of Koplik and co-workers [17] represents the only contribution that we were able to identify commenting on the validity of employing individual *l*-scale Taylor-Aris parameters within the context of network models.
[46] While the microfluidic devices of interest constitute two-

dimensional networks, the theory developed herein is valid for a network of *any* dimensionality. Three dimensions are chosen strictly for the sake of definiteness.

[47] B. Bollobas, *Graph Theory: An Introductory Course* (Springer-Verlag, New York, 1979).

[48] Since the macrotransport parameters $\overline{\mathbf{U}}^*$ and $\overline{\mathbf{D}}^*$ are invariant to choice of coordinate system or abstract representation of the physical medium [1], *any* edge orientation will suffice. However, the microscale convection-diffusion equation [cf. Eq. (3.4)] is valid only for $c(j) \geqslant 0$, a convention which does not arise in the continuous theory [1].

[49] Further reductions in computational effort may be effected by specifying certain equation-specific rules for excluding loops from some of the ensuing summations. We eschew such reductions in what follows since they result in overly burdensome notation, obscuring thereby the inherent simplicity of the scheme itself.

[50] Assigning the volume to the vertices, despite the fact that a large portion of the unit cell's interstitial fluid volume may reside within the channels (edges) of the networks of real devices [3], lies counter to the rationale for assigning the volume to the vertices in a previous network model of this type [14]. There, it was assumed that the capillary tubes comprising the network linkages were thin, hence occupying little volume, whereas their intersections occupied large mixing volumes. Although not the case in present circumstances, the assignation of volume during the course of graphically coarse graining the network geometry is at its very nature *ad hoc*. Therefore, the present scheme does not suffer rationally by prohibiting (by convention) the edges from possessing any volume.

[51] The incidence matrix here is opposite in sign from its traditional graph-theoretical definition [47].

[52] C. Berge, *Graphs and Hypergraphs* (American Elsevier, New York, 1973).

[53] The cell index **I** and its position vector counterpart $\mathbf{R_I}$ will be alternately employed in the following, as necessary.

[54] The edge transport parameters are known *exactly* only for the specific case of infinitesimally small particles translating exclusively under the influence of an externally applied force in an isothermal fluid, since the mobility and the animating force are then each independent of position **r** within the channel.

[55] The mixing rule is the only *vertex* transport process accounted for within this discrete model. There exists no fundamental inconsistency between the continuous model, which implicitly includes convective-diffusive solute mixing processes at the channel intersections, and the present discrete model, since all sensible Lagrangian displacements within the system in the latter model are assigned to the vertex-to-vertex displacement processes occurring within the edges of the graph. Consequently, any ''transport'' occurring internally within the vertex results in no net Lagrangian motion on the macroscale, aside from selecting a new edge.

[56] The factor $K(i,j)$ represents the probability of the particle being located within edge j, whereas $1-K(i,j)$ is the probability of the particle remaining within vertex i. This should not be confused with the probability of the particle exiting in one of $j_1, j_2, \ldots, j_k$ of the k edges incident to vertex i.

[57] In contrast to the molecular diffusivity, the volumetric diffusive transport rate $d(j)$ may be zero if an edge is inaccessible to the particle, corresponding to $K(j)=0$.

[58] N. G. van Kampen, *Stochastic Processes in Physics and Chemistry* (North-Holland, New York, 1981).

[59] In what follows, infinite summations effected over discrete variables constitute counterparts of infinite **R**-space quadratures effected over continuous variables employed in generalized Taylor-Aris dispersion analyses of continuous systems [1]. Similarily, the subsequent mathematical manipulations of the resulting sums in Eq. (4.1) constitute discrete counterparts of ''integration by parts'' in quadratures of continuous variables.

[60] W. M. Deen, AIChE J. **33**, 1409 (1987).

[61] The matrices c_{ij} and d_{ij} in the present scheme correspond to transition matrices in classical statistical physics [58].

[62] C. T. Culbertson, S. C. Jacobson, and J. M. Ramsey, Anal. Chem. **70**, 3781 (1998).

[63] B. M. Rush, K. D. Dorfman, H. Brenner, and S. Kim, Ind. Eng. Chem. Res. (to be published).

[64] M. Pagitsas, A. Nadim, and H. Brenner, Physica A **135**, 533 (1986).

[65] An explicit form for the dispersivity D is presented here for completeness. The L-scale dispersivity $\overline{D}^*$ will ultimately prove expressible as the ratio $\overline{D}^*/D$, irrespective of the exact functional form, namely, Eq. (6.3), adopted for D to characterize the l-scale channel dispersion process.

[66] J. Bear, *Dynamics of Fluids in Porous Media* (Elsevier, New York, 1972).

[67] D. L. Koch and J. F. Brady, J. Fluid Mech. **154**, 399 (1985).

[68] S. Kirkpatrick, Rev. Mod. Phys. **45**, 574 (1973).